

REPORT DOCUMENTATION PAGE

Form Approved
OMB No. 0704-0188

Public reporting burden for this collection of information is estimated to average 1 hour per response, including the time for reviewing instructions, searching existing data sources, gathering and maintaining the data needed, and completing and reviewing this collection of information. Send comments regarding this burden estimate or any other aspect of this collection of information, including suggestions for reducing this burden to Department of Defense, Washington Headquarters Services, Directorate for Information Operations and Reports (0704-0188), 1215 Jefferson Davis Highway, Suite 1204, Arlington, VA 22202-4302. Respondents should be aware that notwithstanding any other provision of law, no person shall be subject to any penalty for failing to comply with a collection of information if it does not display a currently valid OMB control number. PLEASE DO NOT RETURN YOUR FORM TO THE ABOVE ADDRESS.

1. REPORT DATE (DD-MM-YYYY)		2. REPORT TYPE Technical Papers		3. DATES COVERED (From - To)	
4. TITLE AND SUBTITLE				5a. CONTRACT NUMBER	
				5b. GRANT NUMBER	
				5c. PROGRAM ELEMENT NUMBER	
6. AUTHOR(S)				5d. PROJECT NUMBER 2303	
				5e. TASK NUMBER M2C8	
				5f. WORK UNIT NUMBER	
7. PERFORMING ORGANIZATION NAME(S) AND ADDRESS(ES)				8. PERFORMING ORGANIZATION REPORT	
Air Force Research Laboratory (AFMC) AFRL/PRS 5 Pollux Drive Edwards AFB CA 93524-7048					
9. SPONSORING / MONITORING AGENCY NAME(S) AND ADDRESS(ES)				10. SPONSOR/MONITOR'S ACRONYM(S)	
Air Force Research Laboratory (AFMC) AFRL/PRS 5 Pollux Drive Edwards AFB CA 93524-7048				11. SPONSOR/MONITOR'S NUMBER(S)	
12. DISTRIBUTION / AVAILABILITY STATEMENT					
Approved for public release; distribution unlimited.					
13. SUPPLEMENTARY NOTES					
14. ABSTRACT					
1121 036					
15. SUBJECT TERMS					
16. SECURITY CLASSIFICATION OF:			17. LIMITATION OF ABSTRACT	18. NUMBER OF PAGES	19a. NAME OF RESPONSIBLE PERSON Leilani Richardson
a. REPORT		b. ABSTRACT	c. THIS PAGE	A	19b. TELEPHONE NUMBER (include area code) (661) 275-5015
Unclassified		Unclassified	Unclassified		62

TP-FY99-0107

✓ Spreadsheet
✓ DB

MEMORANDUM FOR PRR (In-House Publication)

24 May 1999

FROM: PROI (TI) (STINFO)

SUBJECT: Authorization for Release of Technical Information, Control Number: AFRL-PR-ED-TP-FY99-0107
Bill Larson, "Identification and Condensation of Cyclic C₆ and Cyclic C₈ in Solid Argon and Matrix-Isolated
Boron/Carbon"

(Public Release)

Presentation

Identification and condensation of cyclic C₆ and cyclic C₈ in solid argon

Characterization of matrix isolated B_JC_{n-J} J=0, 1, 2; n=3-11 in solid argon

C. William Larson
Propulsion Directorate
Air Force Research Laboratory
Edwards AFB, CA 93524-7680

HEDM RESEARCH GROUP

Pat Carrick (Chief), Jeff Sheehy (Group Leader), Greg Drake, Hi Young Yoo, Jeffrey Mills, Jerry Boatz,
Jessica Harper, Karl Christe, Mario Fajardo, Michael Tinnirello, Michelle DeRose, Paul Jones,
Txomin Presilla (Schafer Corporation) Peter Langhoff, Simon Tam, Suresh Suri, William Wilson ✓

University of Florida
Department of Chemistry
Gainesville, Florida
June 8, 1999

20021121 036

Rocket Science

$$\frac{m_{final}}{m_{initial}} = \exp - \frac{\Delta V}{g I_{sp}}$$

$$I_{sp} = \frac{1}{g} \sqrt{2(h_{propellant} - h_{exit})}$$

h = enthalpy per unit mass

*Is there a point
to this chart?
a relationship
between 1st & 2nd
of that is relevant?*

DISTRIBUTION STATEMENT A
Approved for Public Release
Distribution Unlimited

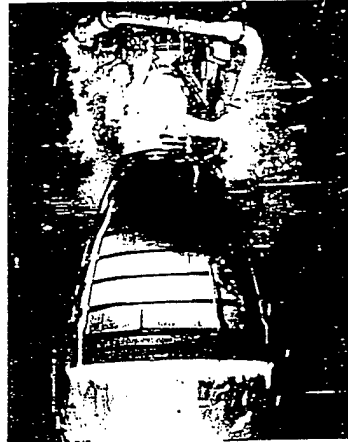
SSME

Rockwell International
Rockeydyne Division

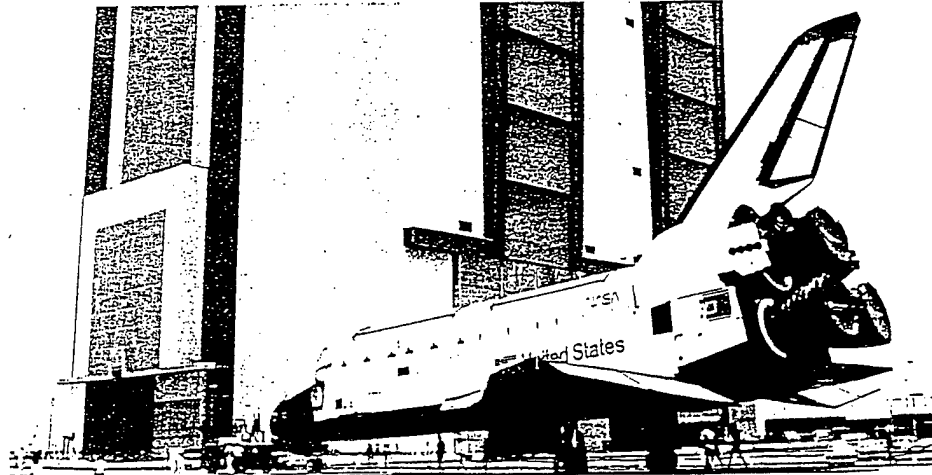
SPACE SHUTTLE MAIN ENGINE

The Space Shuttle Main Engine (SSME) was developed expressly for use on America's Space Shuttle. Using a mixture of liquid oxygen and liquid hydrogen, the SSME can attain a maximum thrust level (in vacuum) of 512,300 pounds at 109% power level. The regeneratively cooled engine also features high performance turbopumps for propellant and oxidizer that develop 77,310 horsepower and 29,430 horsepower, respectively. Ultra-high-pressure operation of the pumps and combustion chamber allows expansion of all hot gases through a high-area-ratio exhaust nozzle to achieve efficiencies never previously attained in a production rocket engine. These advantages allow a heavier payload to be carried without increasing launch vehicle size.

SPACE SHUTTLE MAIN ENGINE PERFORMANCE (FULL POWER LEVEL)

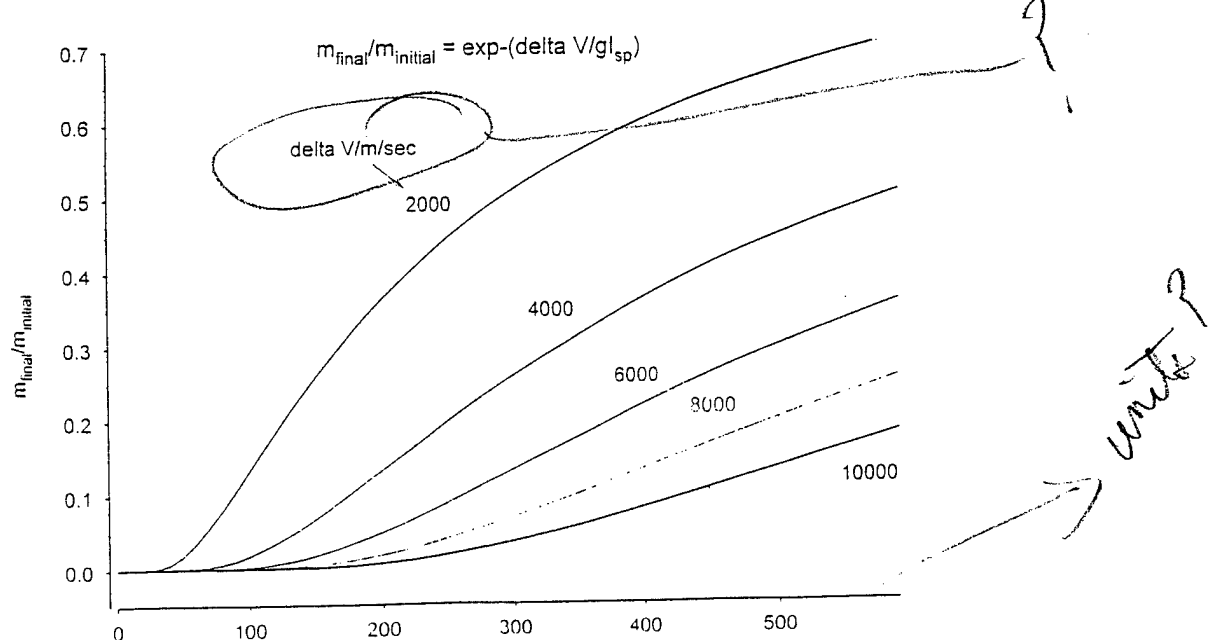


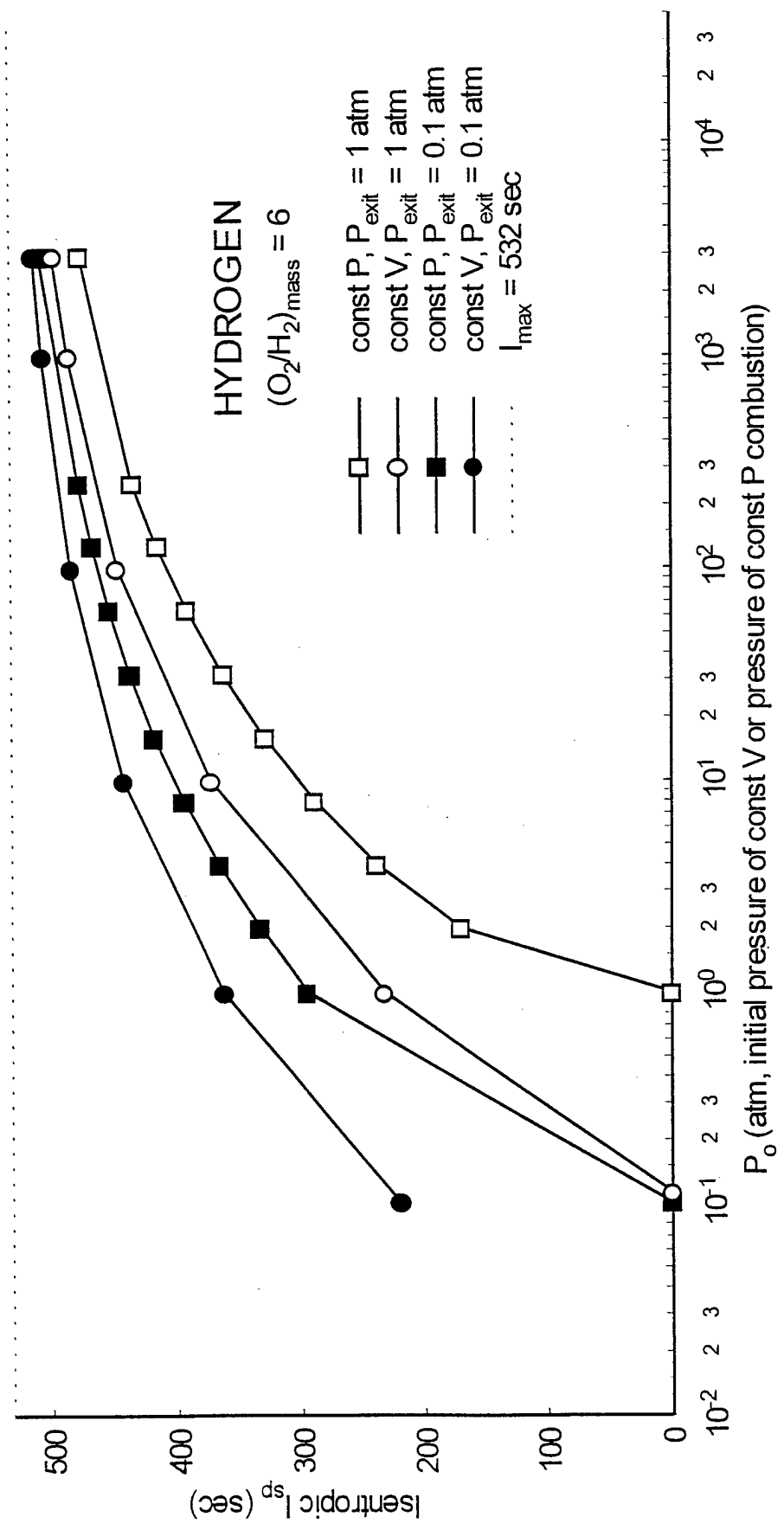
Maximum Thrust: (109% Power Level)		
At Sea Level	408,750 pounds	
In Vacuum	512,300 pounds	
Throttle Range	65% ~ 109%	
Pressures:		
Hydrogen Pump Discharge	7,040 psia	
Oxygen Pump Discharge	8,070 psia	
Chamber Pressure	3,260 psia	
Specific Impulse (In Vacuum)	4,444 km/s, 453.5 seconds	
Power: 5.07 GW (E _{net} , in vacuum)		
High Pressure Pumps		
Hydrogen	77,310 horsepower	
Oxygen	29,430 horsepower	
Area Ratio	77.5:1	
Weight:	6,367 x 10 ³ kg/N	
Mixture Ratio (O/F)	6.0:1	
Dimensions:	168 in. long/96 in. wide	
Propellants:		
Fuel	Liquid Hydrogen	
Oxidizer	Liquid Oxygen	



For more information contact: ELV Propulsion/Rockwell International/Rocketdyne Division/6633 Canoga Ave./
Canoga Park/CA/91303/(818)700-6027

Pub. 571-M-80b New 1-7





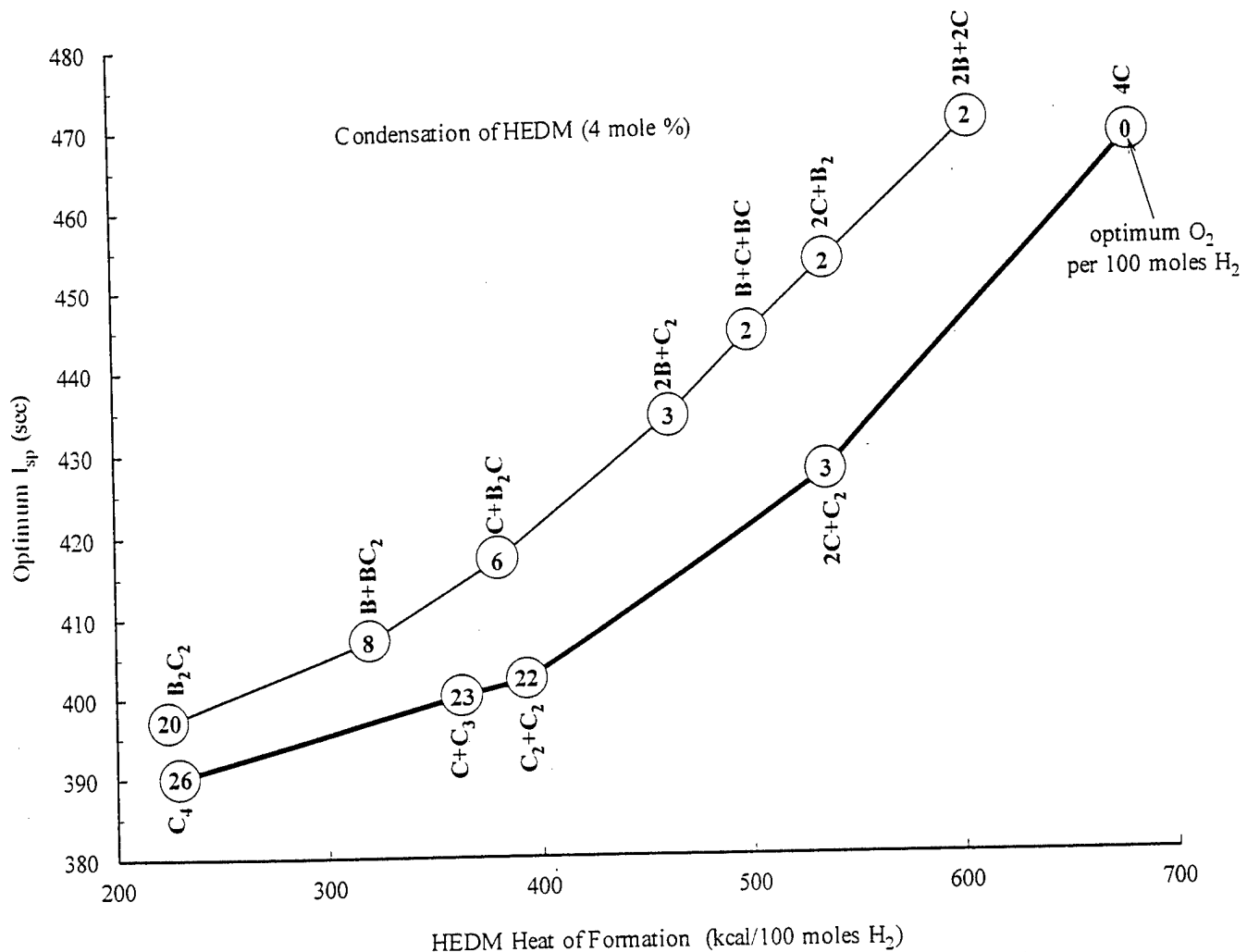


Figure 1. Specific impulse of HEDM containing 4 mole percent equivalent atom density in solid hydrogen with various stages of condensation. Numbers inside circles denote the optimum moles of O_2 per 100 moles of H_2 that produces the maximum I_{sp} for the indicated compositions. The calculations are based on the standard rocket operating conditions, 1000 psi combustion pressure and 1 atm nozzle exit pressure, which produce 389 sec with liquid oxygen/liquid hydrogen propellant. The propellant composed of 4 mole percent C-atoms produces maximum I_{sp} with no oxygen. If the atoms condense to 1 mole percent C_4 , the I_{sp} drops to the baseline 389 sec value.

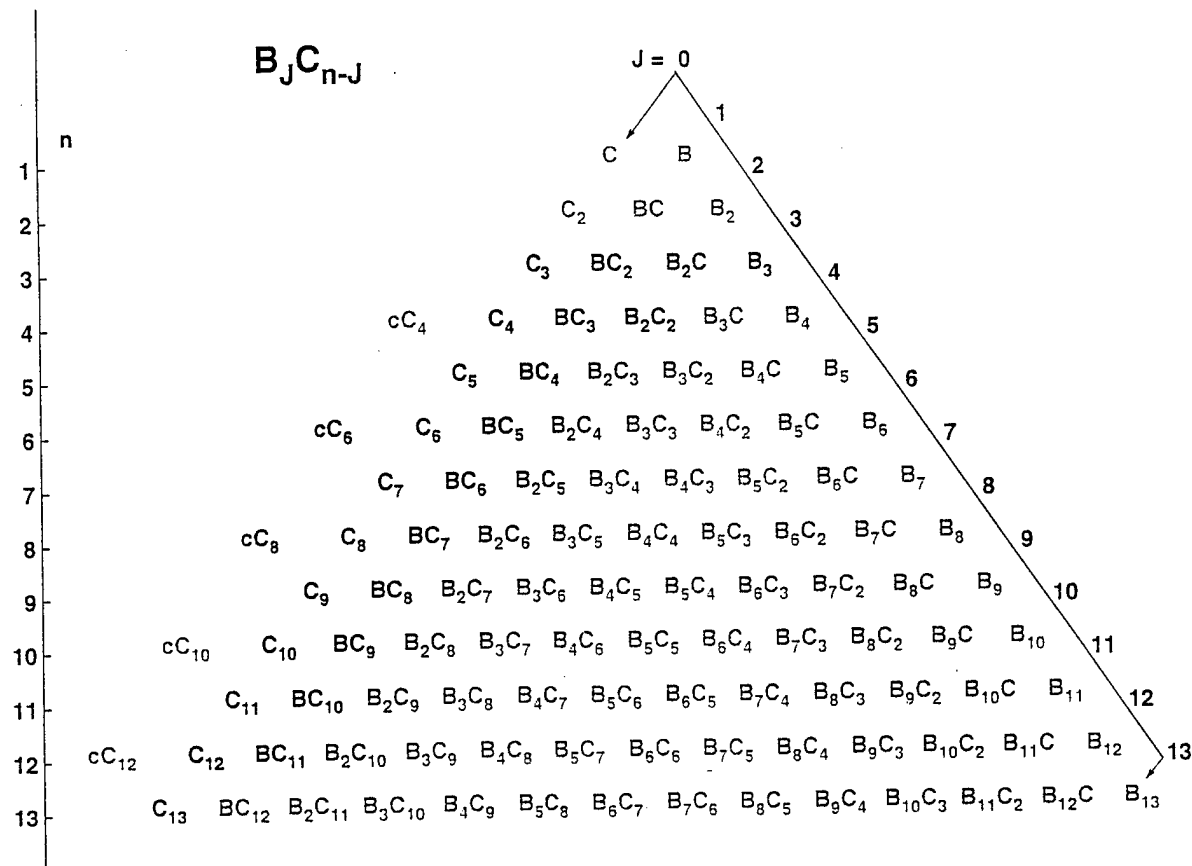
Objective - 5% atoms in cryogenic matrix

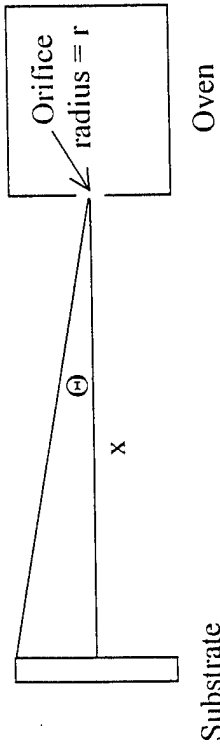
Approach

1. FTIR spectroscopy of $B_J C_{n-J}$ clusters isolated in 10 K argon matrix
2. Ab-initio calculations of cluster
 - (a) normal mode frequencies and frequency shifts of their isotopomers
 - (b) infrared absorption intensities (km mol^{-1})
3. Measurement of cluster distributions produced upon deposition and after annealing. Absolute column densities (molecules cm^{-2}) from Beer's Law

$$\langle \rho_i I \rangle = \frac{A_{\text{exp}}}{I_{\text{theory}}} N$$

$$A_{\text{exp}} = - \int_v \ln \left[\frac{E_t(v)}{E_0(v)} \right] dv$$





$$(1) \quad Q_{\text{atom}}(\Theta, x) = \frac{1}{4} \rho \bar{c} a \frac{\cos^3 \Theta}{\pi x^2}$$

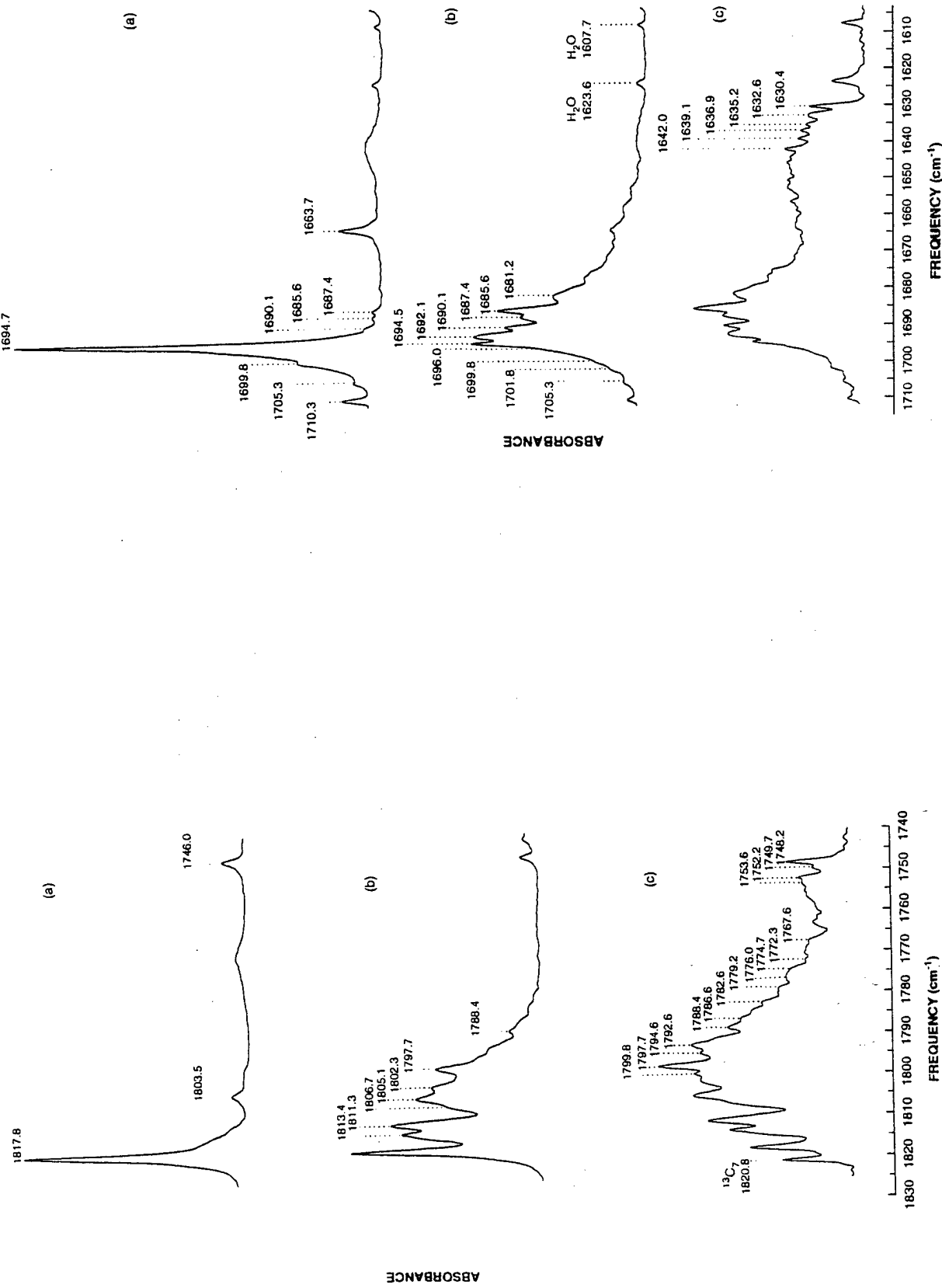
$$(2) \quad Q_{\text{rad}}(\Theta, x) = \sigma T^4 a \frac{\cos^3 \Theta}{\pi x^2}$$

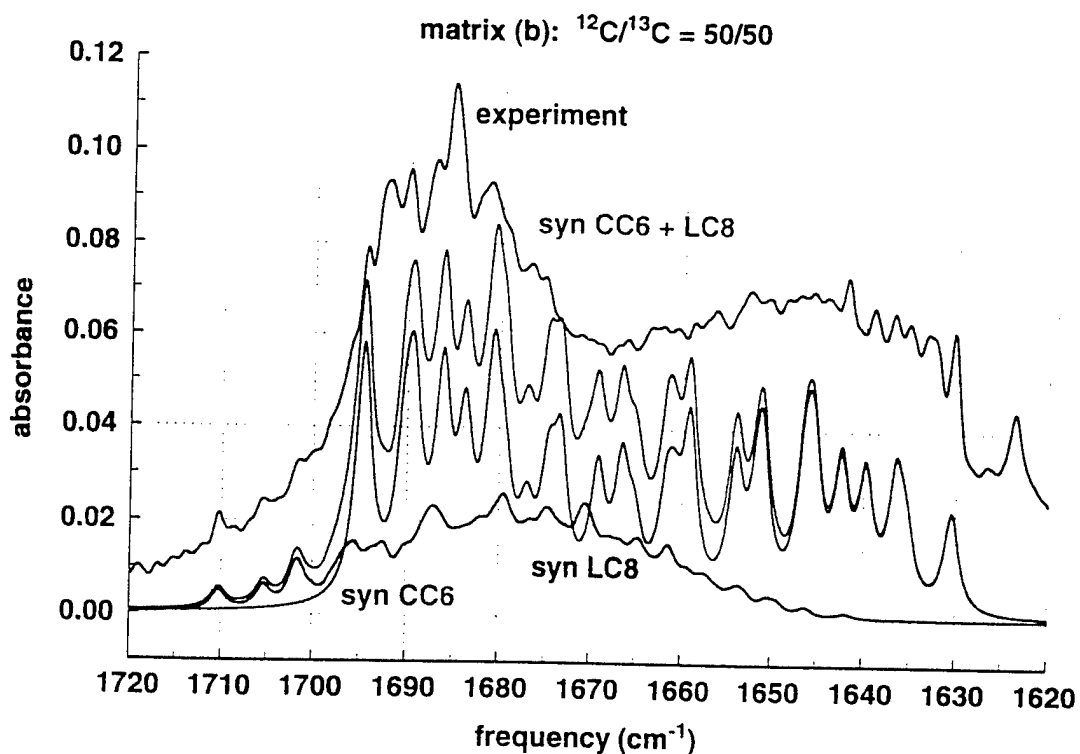
Table I. Properties of a boron evaporation oven^(a), $r = 0.05$ cm, $\theta = 0$

θ	$x = 10$ cm			$x = 20$ cm
	0.01	0.1	1	10
P (Torr)				
T (K)	2409	2631	2898	3230
ρ (#/cm ³)	4.01×10^{13}	3.67×10^{14}	3.33×10^{15}	2.98×10^{16}
\bar{c} (cm/s)	2.13×10^5	2.24×10^5	2.35×10^5	2.48×10^5
Evap rate (#/s)	1.68×10^{16}	1.61×10^{17}	1.53×10^{18}	1.45×10^{19}
Evap rate (mg/hour)	1.11	10.6	101	957
λ (cm) ^(b)	100.0	10.9	1.20	0.134
$K_n = \lambda/2r$	1000	109	12.0	1.34
Q_{atom} (#/cm ² s)	5.37×10^{13}	5.13×10^{14}	4.89×10^{15}	1.17×10^{16}
Q_{rad} (mW/cm ²)	4.74	6.75	9.93	3.78

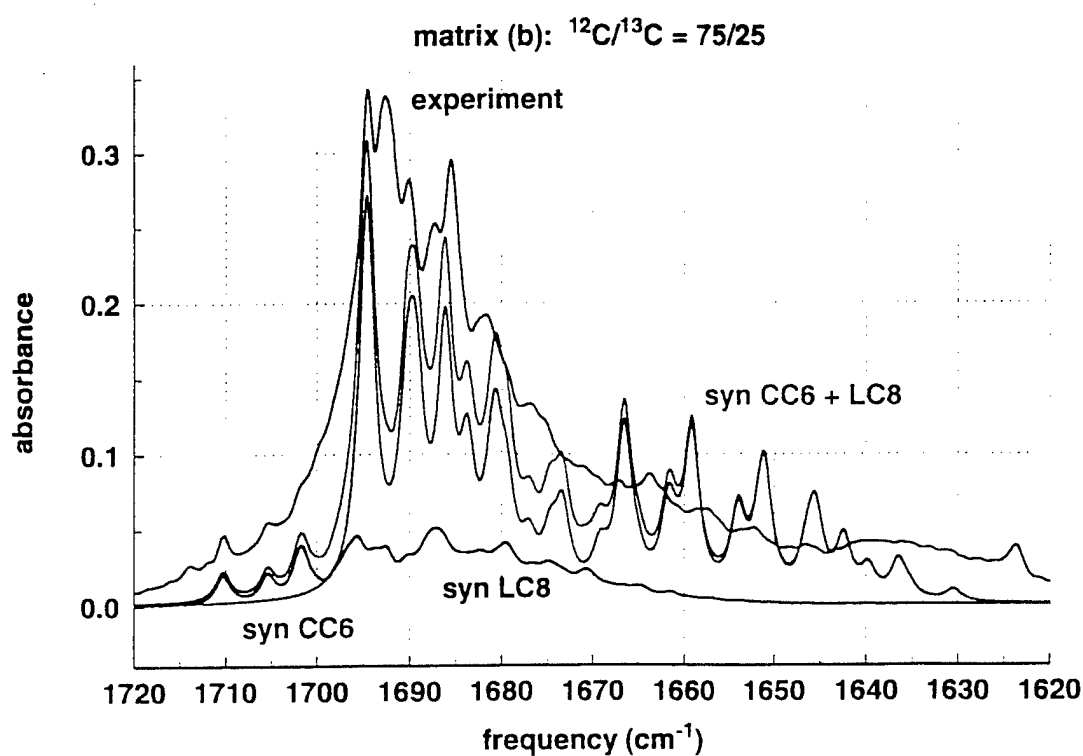
(a) Based on vapor pressure data from Nesmeyanov's (1963) compilation, "Vapor Pressure of the Elements."

(b) Mean free path based on a collision diameter of 1.59×10^{-8} cm for boron + boron [Moelwyn-Hughes (1961), p25].

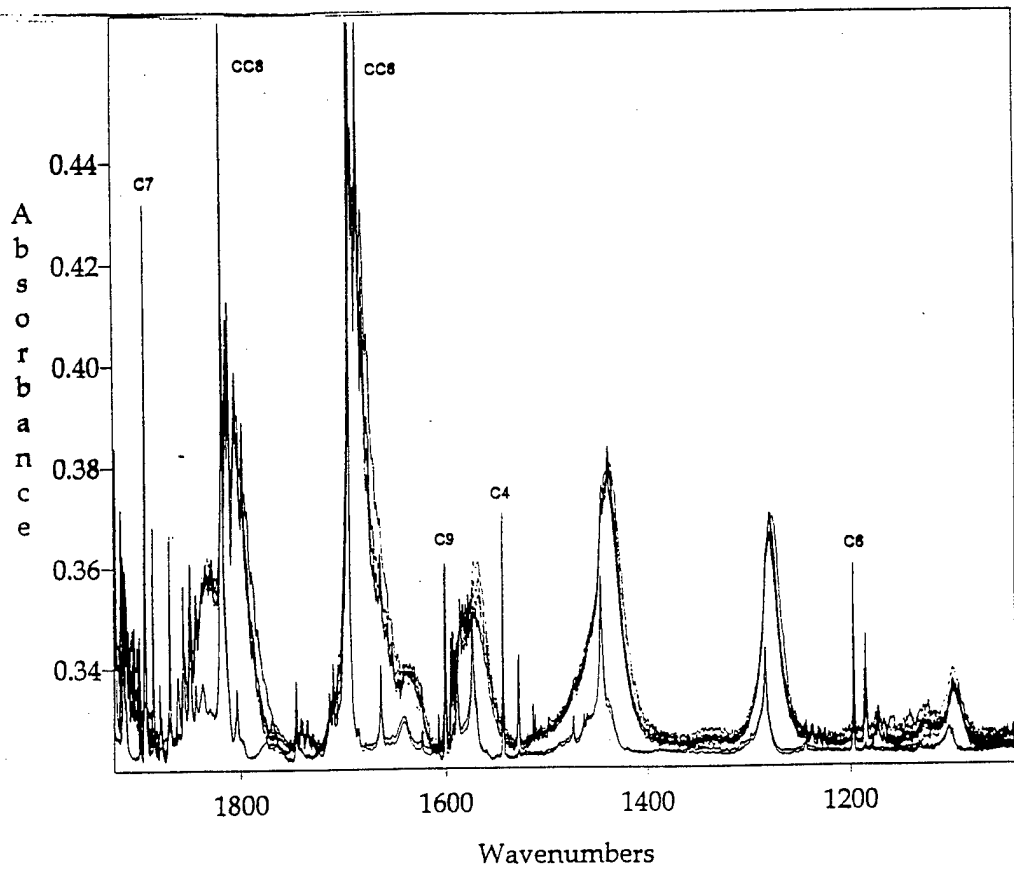
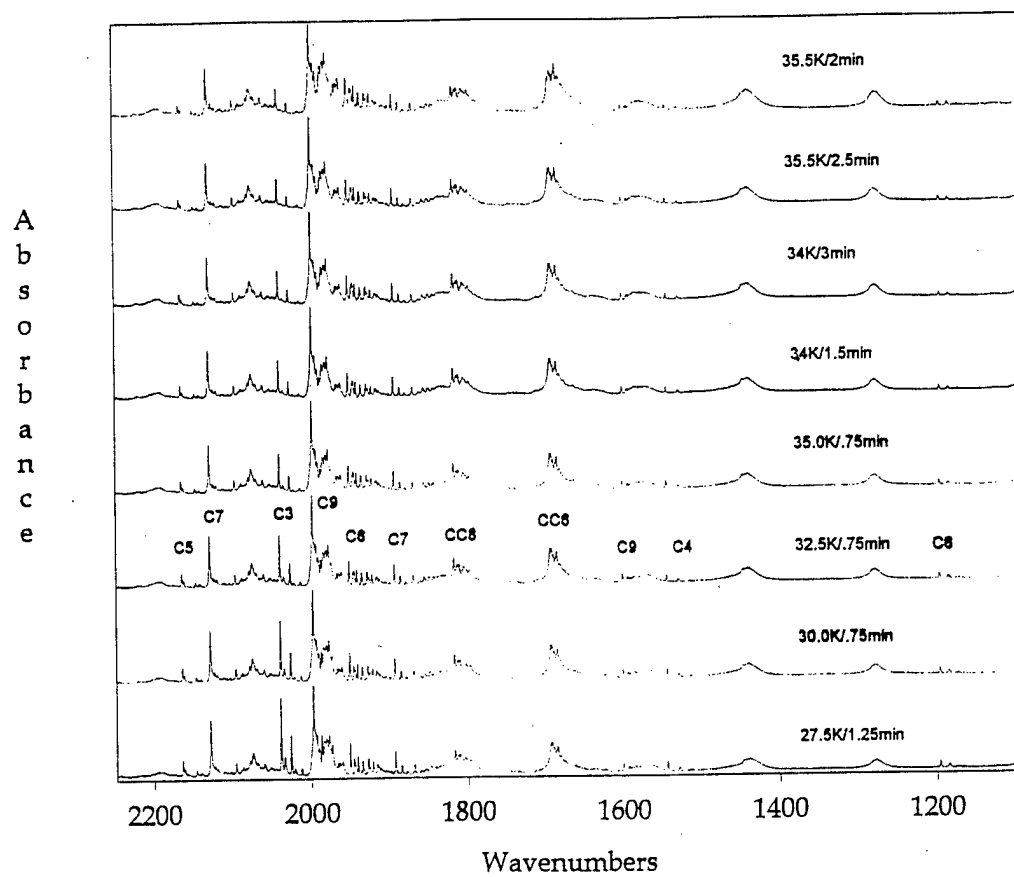


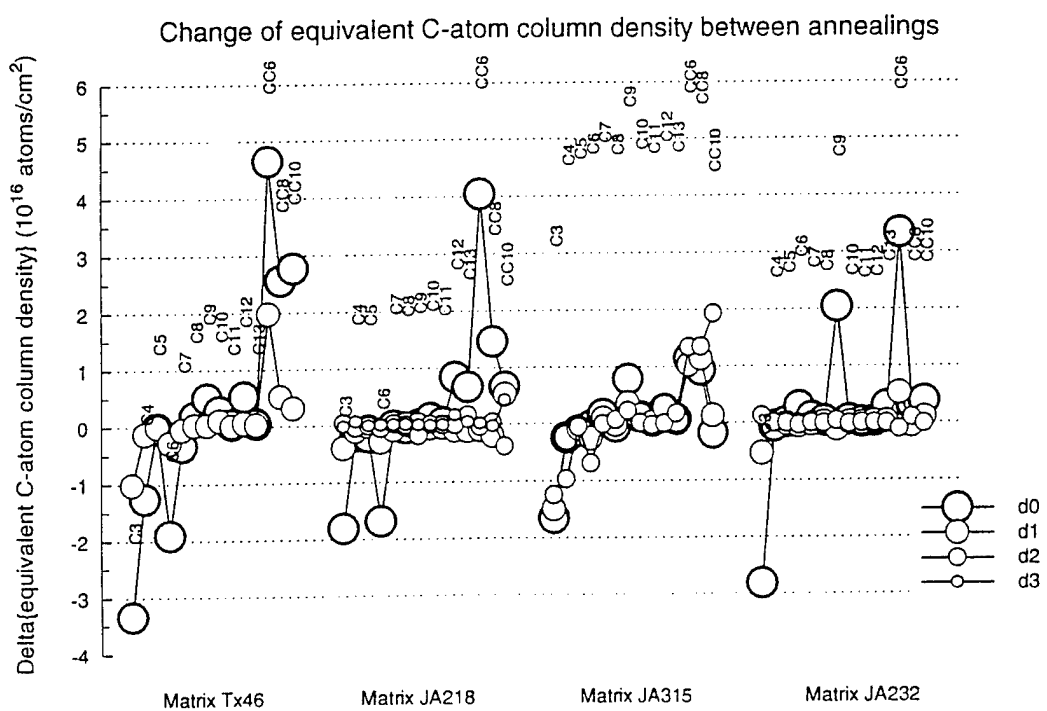
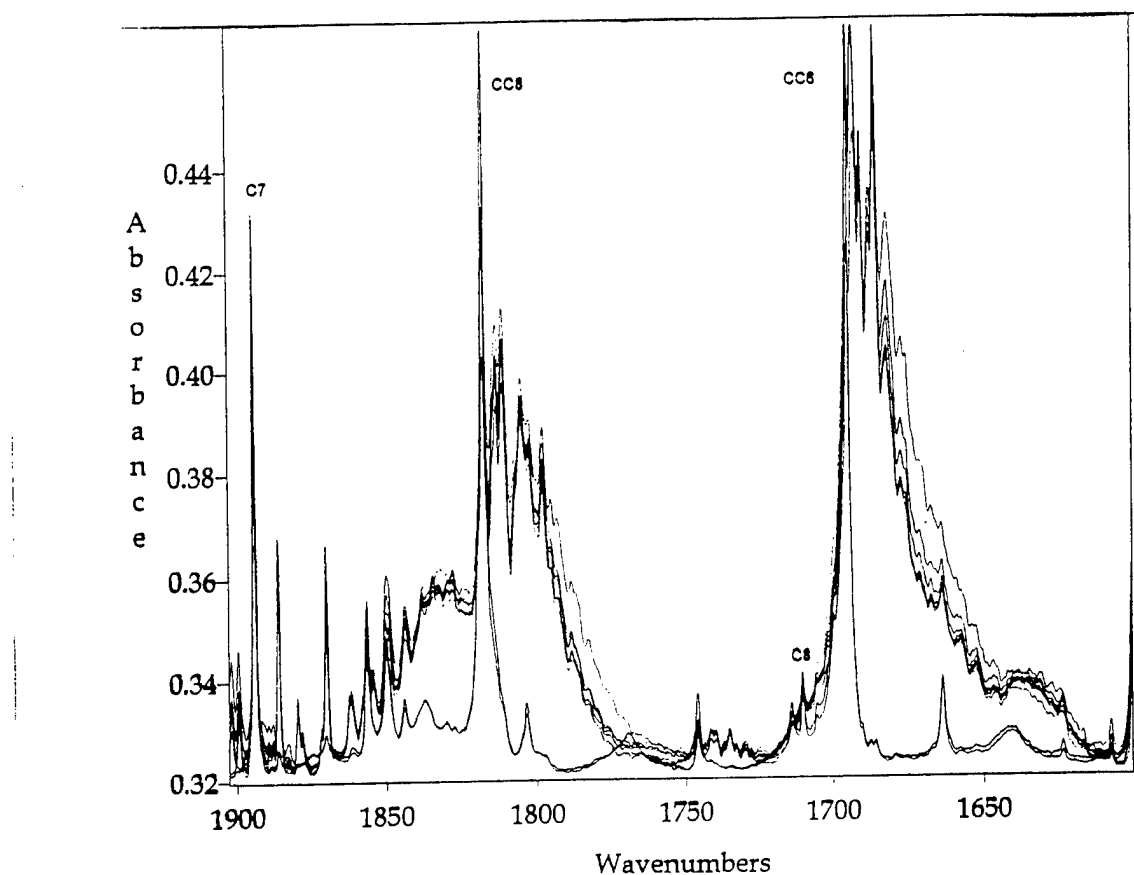


syncerGB.dat

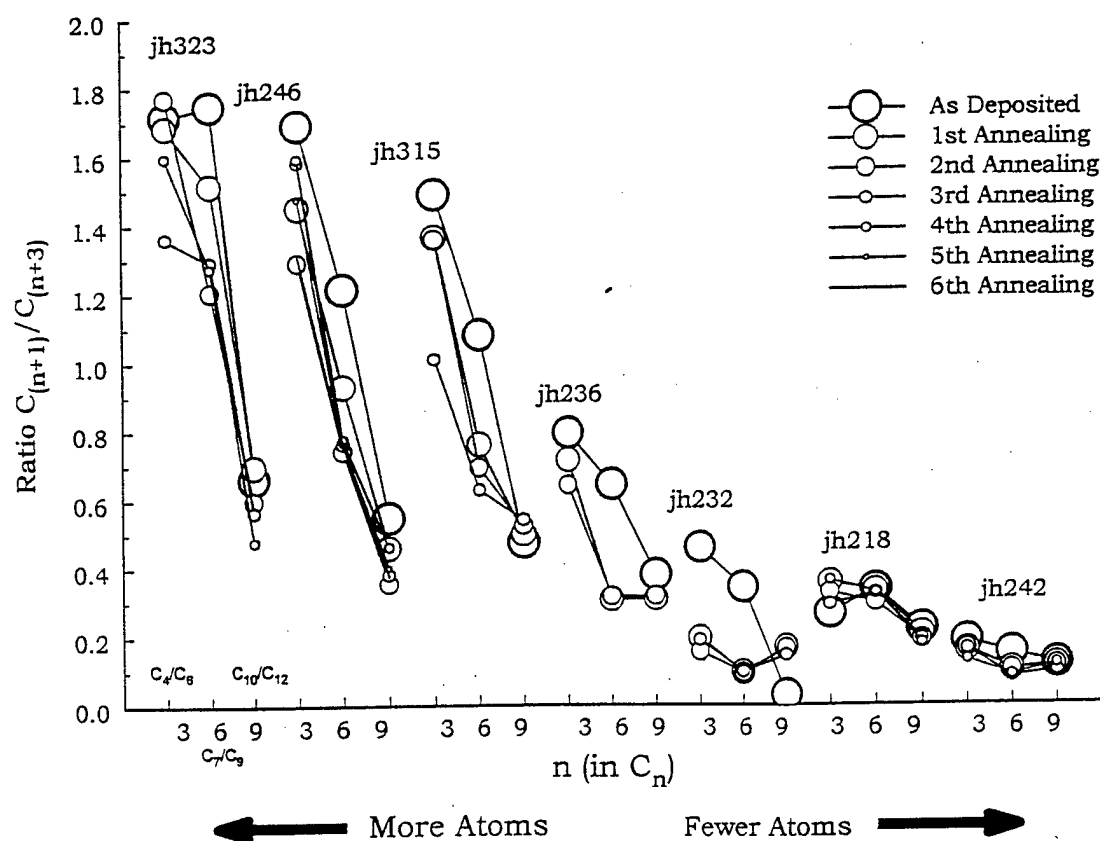


syncerGB.dat





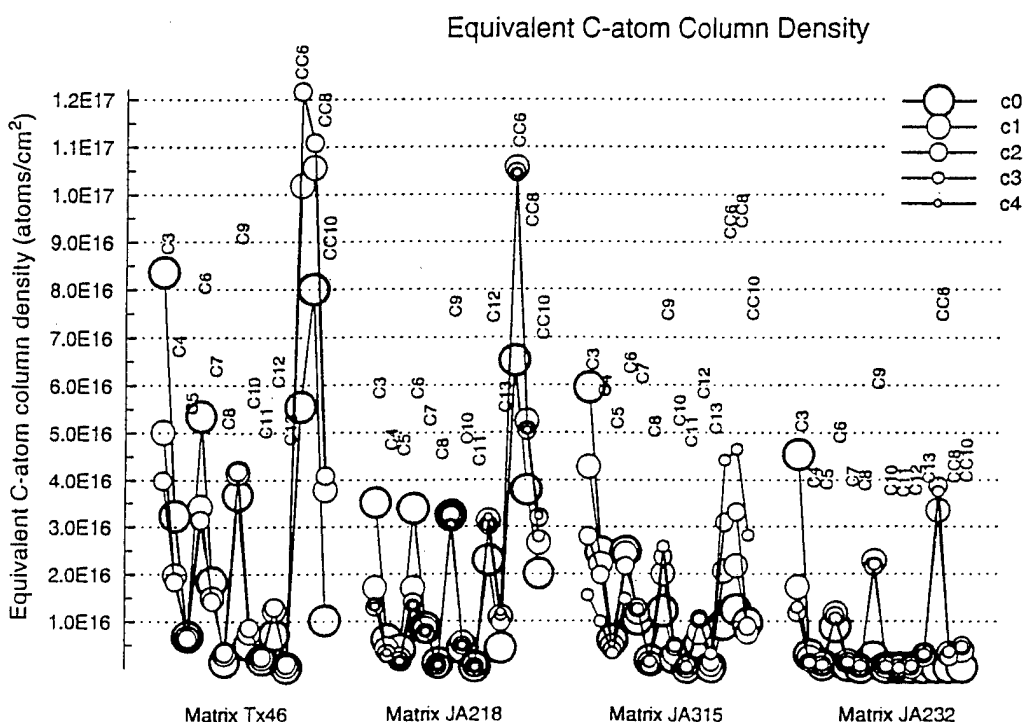
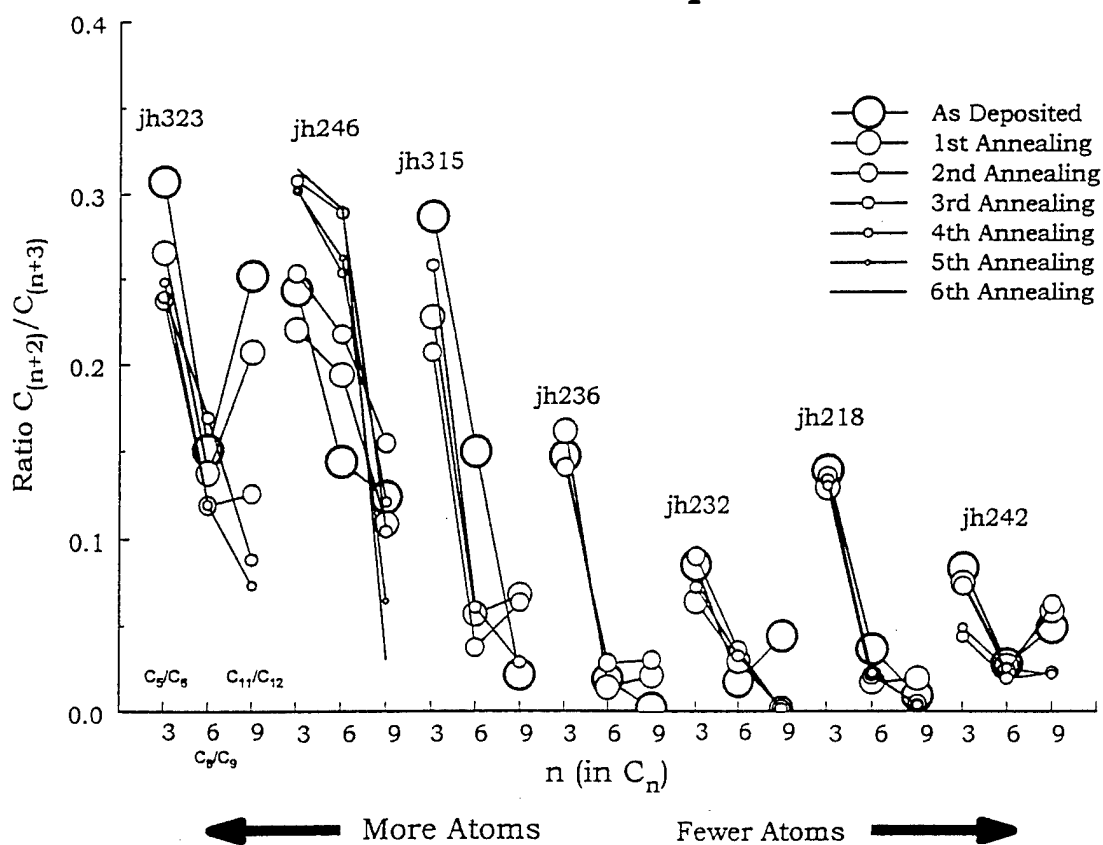
Comparison of C_4/C_6 , C_7/C_9 , C_{10}/C_{12} Ratios Obtained for Different Experimental Conditions



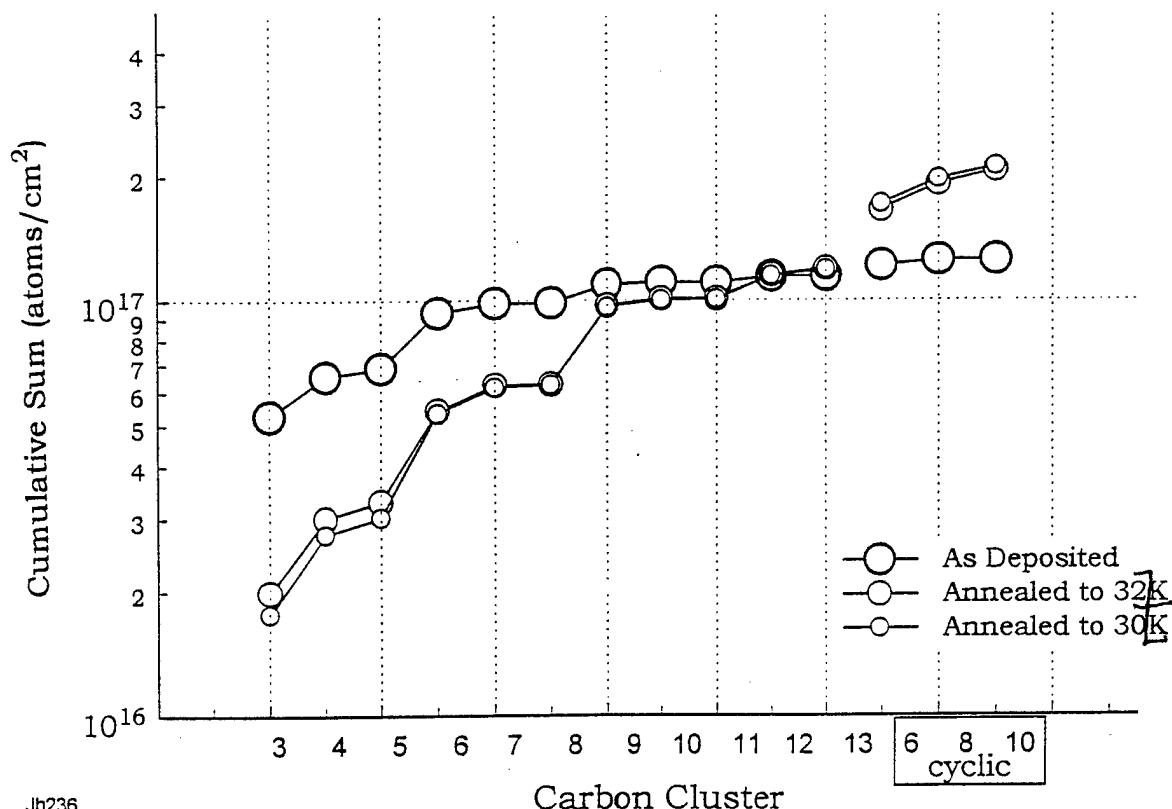
The ratio of the equivalent carbon atom column density for $n+1$ species (n as in C_n) to the equivalent carbon atom column density for $n+3$ species indicates how many atoms were available for formation of species like C_4 , C_7 , and C_{10} . When the Ta cell was hotter more $n+1$ species were formed during deposition than when the cell was colder. During annealings there were only minimal changes in the relative order of the ratios for C_4/C_6 ; C_7/C_9 ; C_{10}/C_{12} . Similar results are noted for $C(n+2)/C(n+3)$.

The run with 5% H_2 /95% Ar yields a lower $C(n+1)/C(n+3)$ ratio than would be expected. The hydrogen may be scavenging atoms.

Comparison of C_5/C_6 , C_8/C_9 , C_{11}/C_{12} Ratios Obtained for Different Experimental Conditions



Cumulative Sum of Equivalent Carbon Atom Density



Jh236

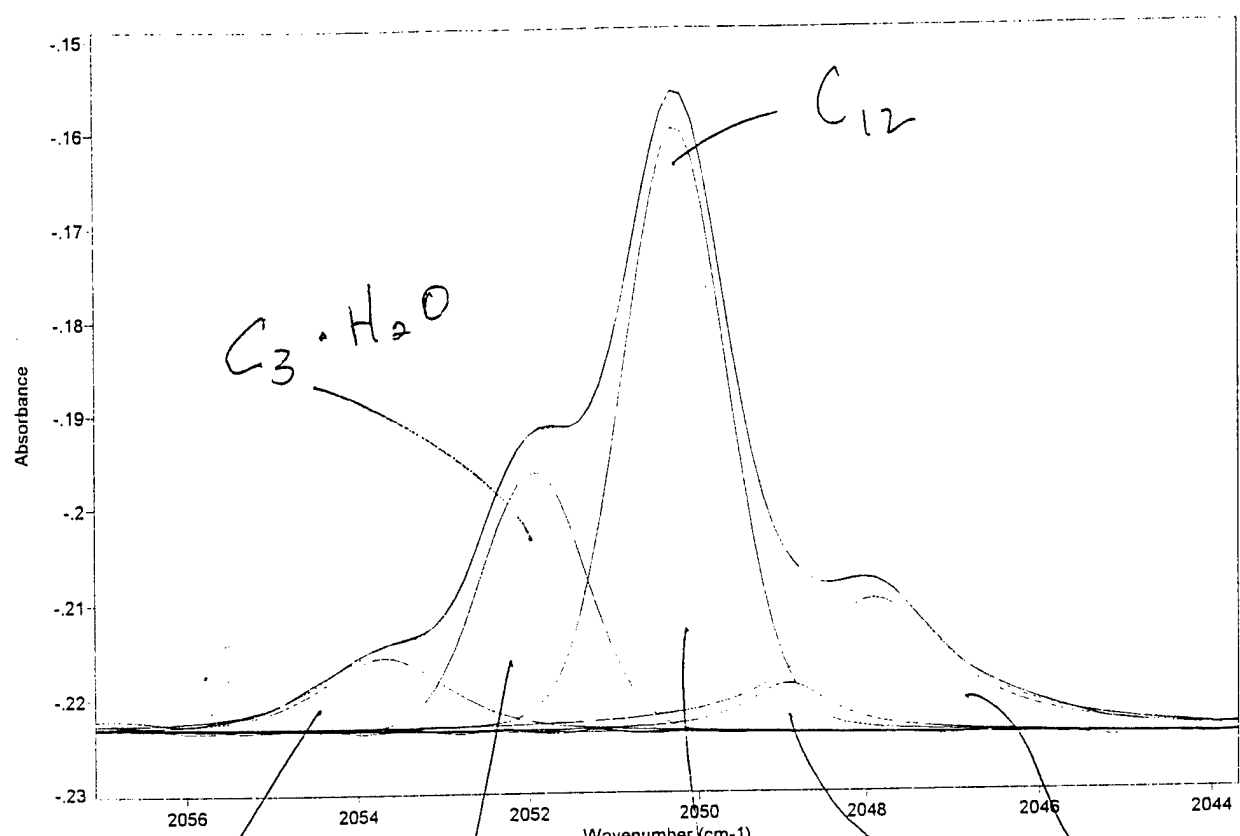
Jh236ord4.ppt May 15 1998 12:40:39 PM

From successive cluster distributions one can calculate the quantity of carbon species that were not detected in the as-deposited matrix IR spectrum. This increase in the total equivalent carbon atom density is attributed to carbon atoms that are "invisible" to IR and were thus not accounted for in the original IR spectrum.

1= MixG+L (2053.7, .0078452, 1.7666, .44691)
4= MixG+L (2048.9, .0052507, 1.2237, .99803)

2= MixG+L (2051.9, .027381, 1.4388, 1.00E-06)
5= MixG+L (2047.9, .014253, 1.9605, .99103)

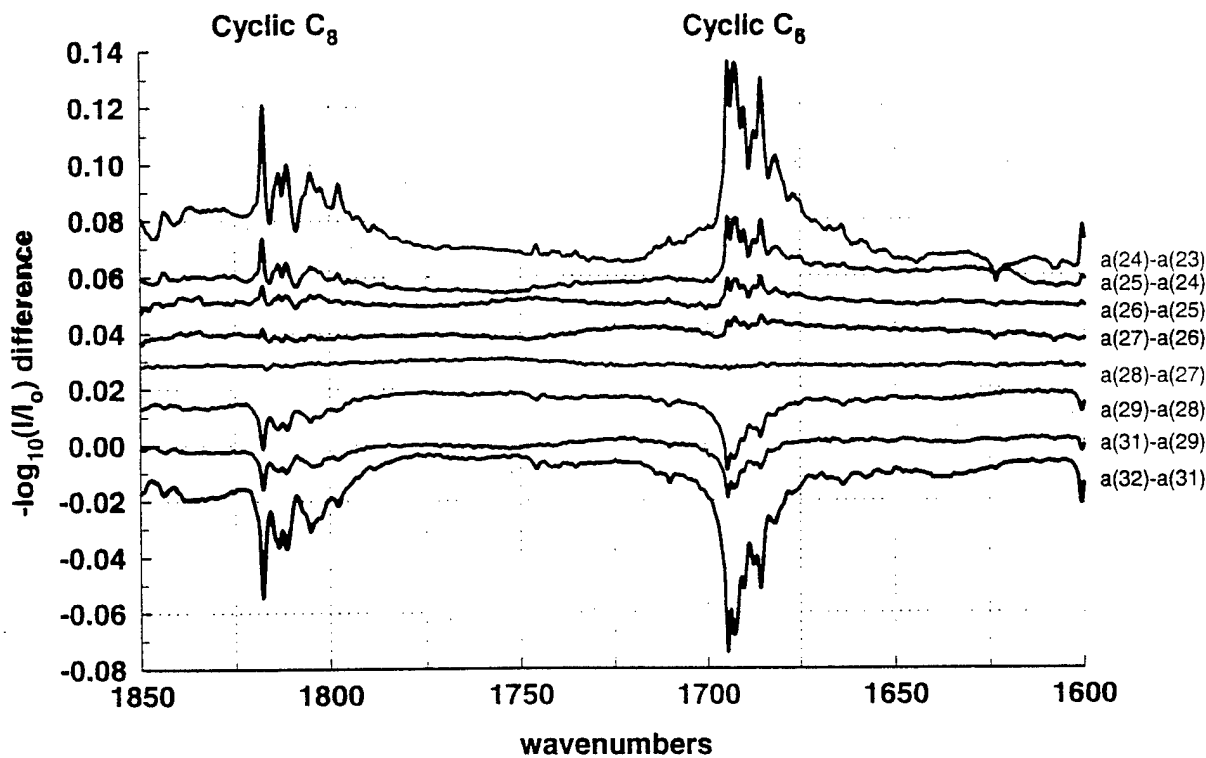
3= MixG+L (2050.3, .064283, 1.434, .10607)
6= Quadr (-.41118, .000086926, 2.15E-09)



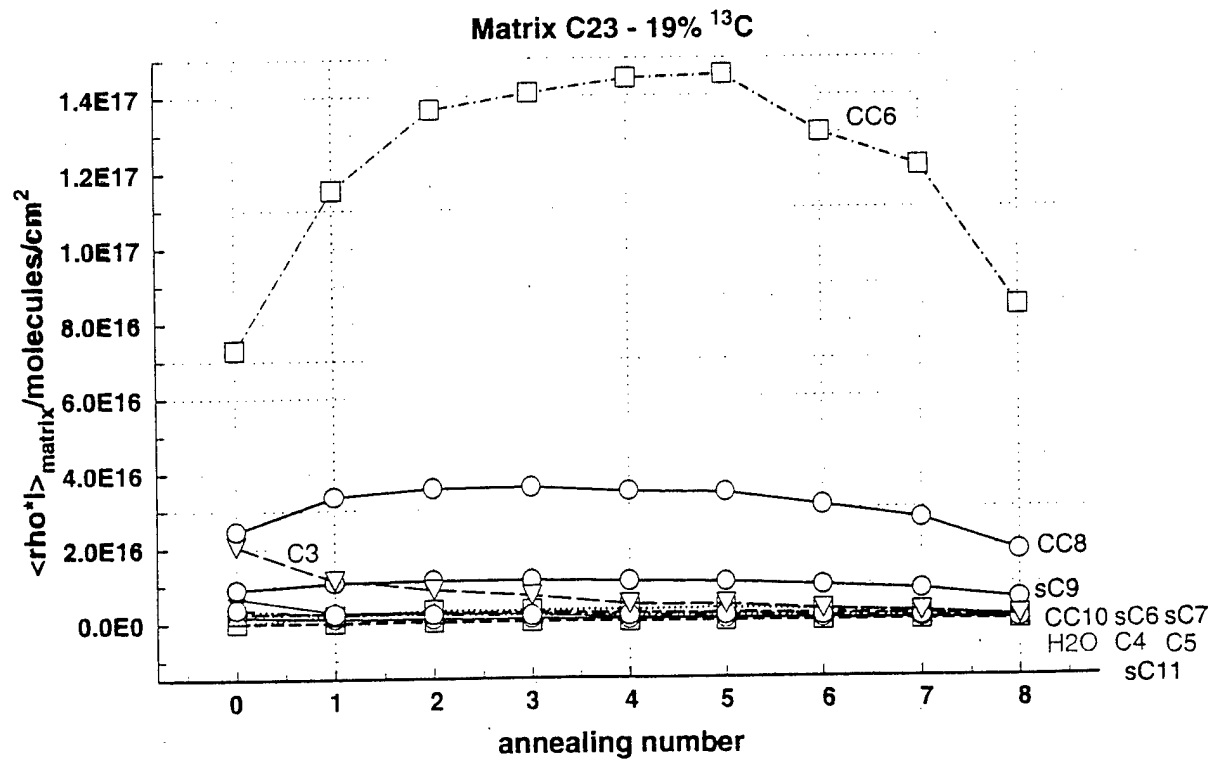
$\lambda =$ 2053.7
Peak # → 1
width → 1.7
% Lorentzian → 44%
Peak # → 2 1.4
width → 0%
% Lorentzian → 0%
Peak # → 3 1.4
width → 100%
% Lorentzian → 100%
Peak # → 4 1.2
width → 99%
% Lorentzian → 99%
 $\lambda =$ 2051.9
 $\lambda =$ 2050.3
 $\lambda =$ 2048.9
 $\lambda =$ 2047.9

Hanna Resler -
cal of w/Wtng (3f)

Matrix C23

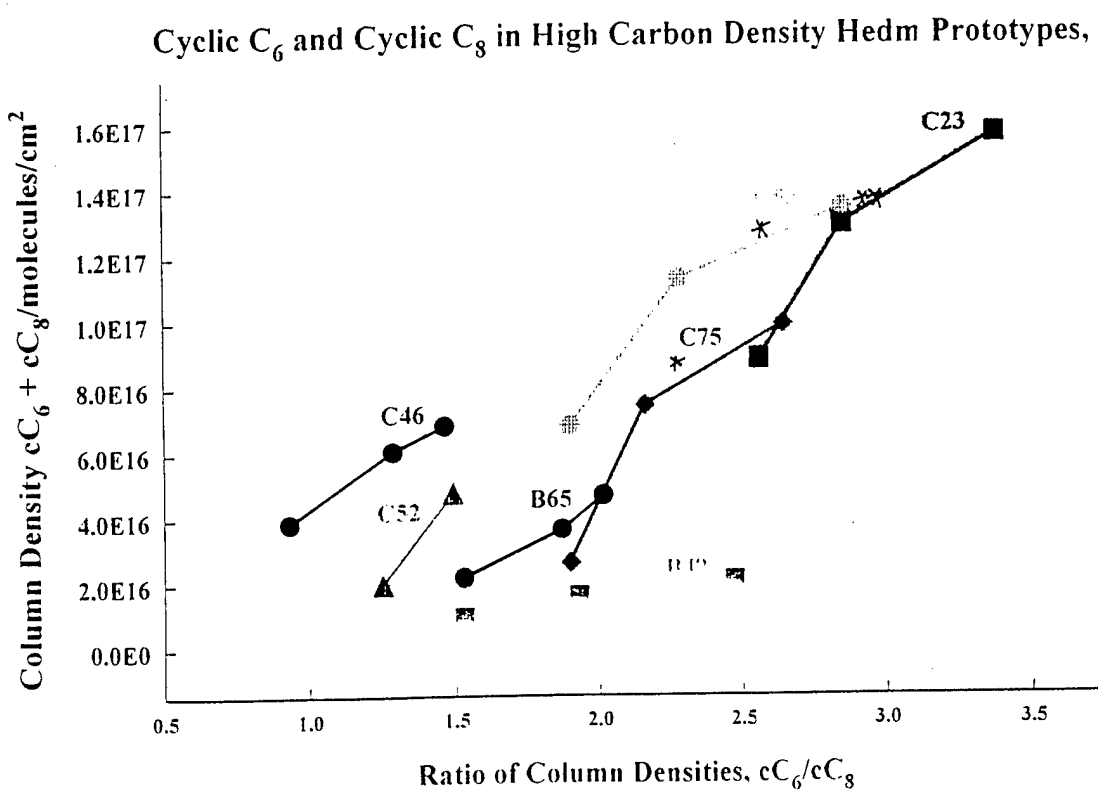
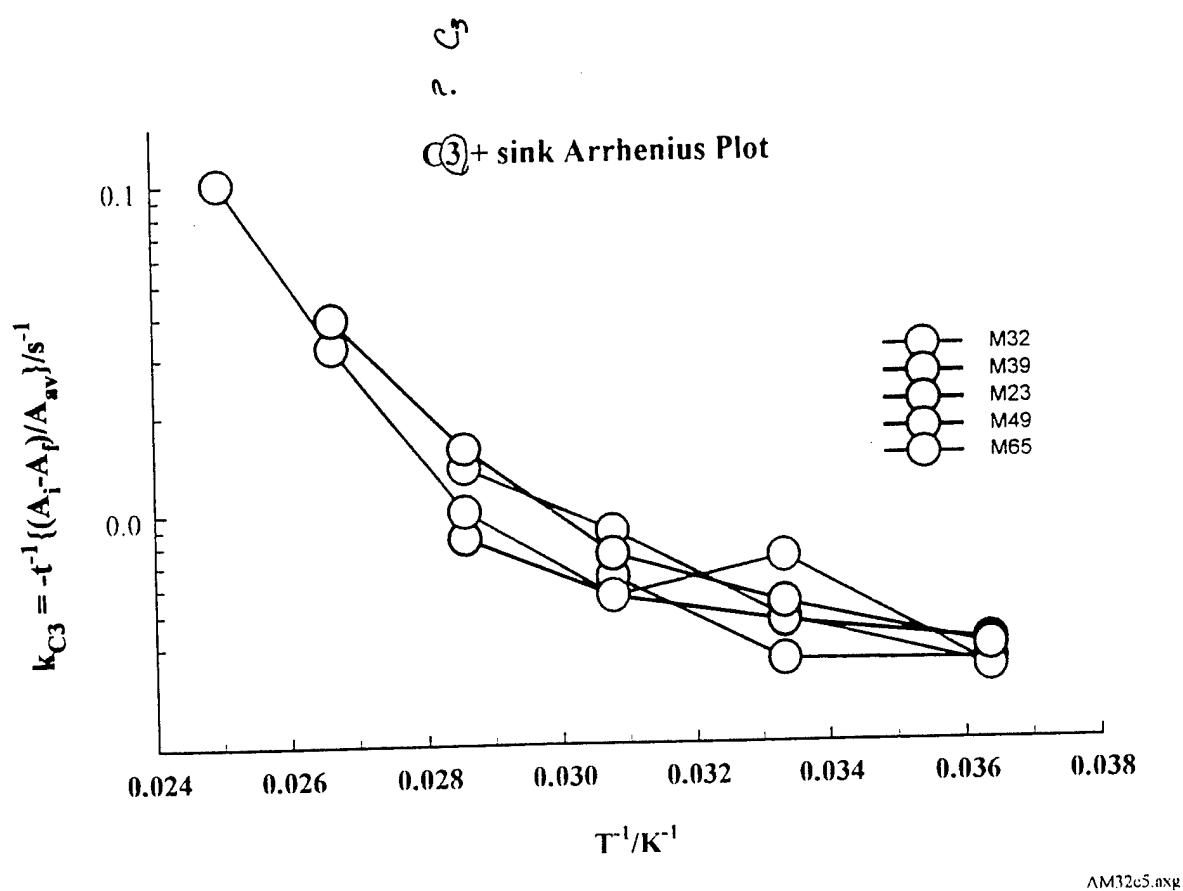


c6dif233.axg Phillips Lab, Edwards AFB, CA 93524 Sept. 11, 1997 3:15:09 PM



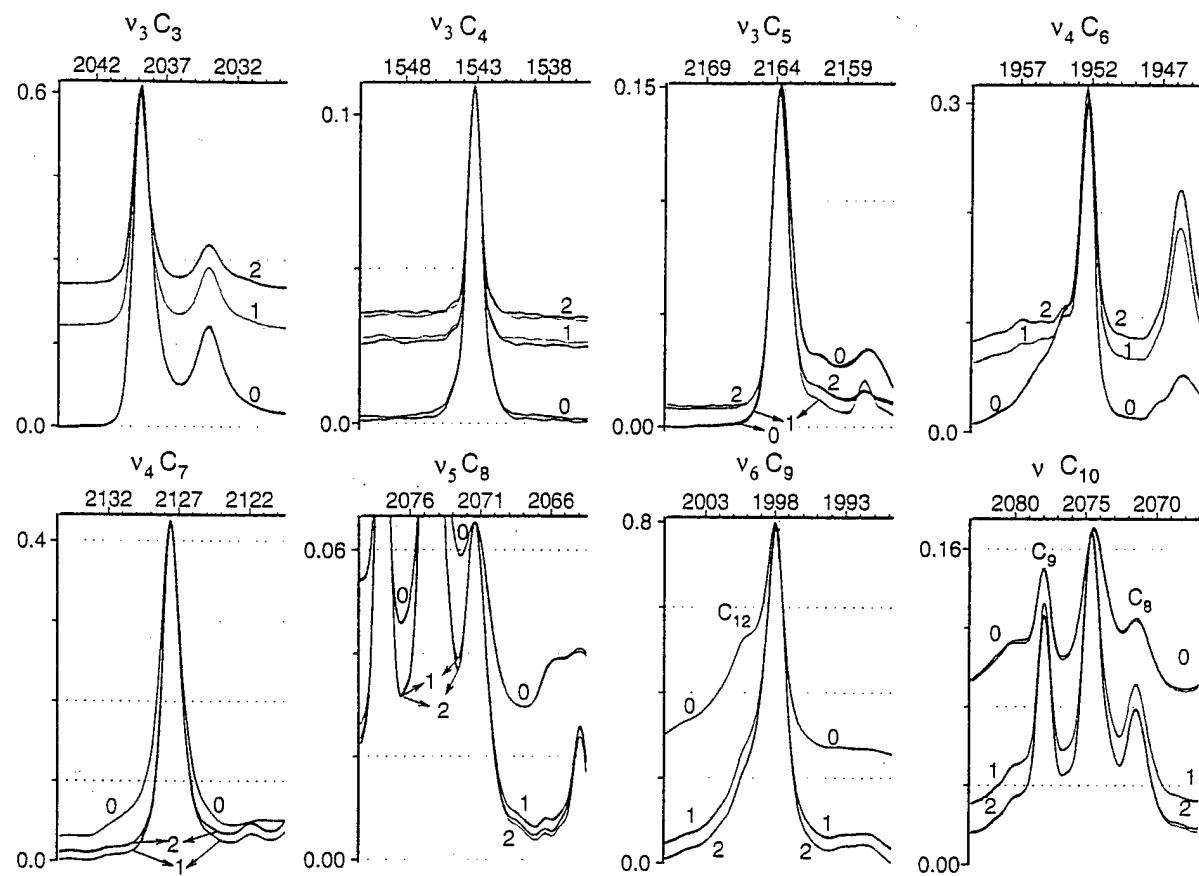
C23c2a.axg

15

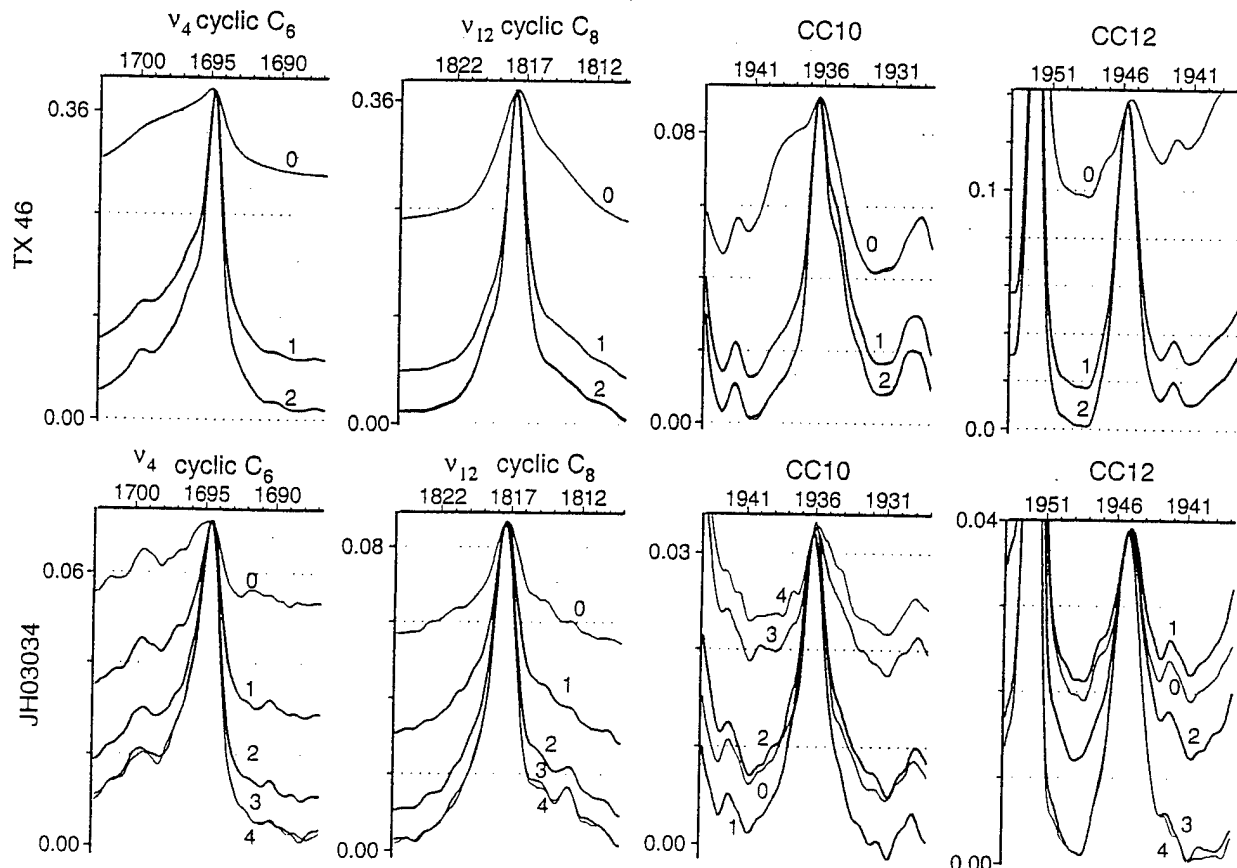


MhiDsmly1.oxg

(6)



Carbon Matrix (a) - C_n Clusters



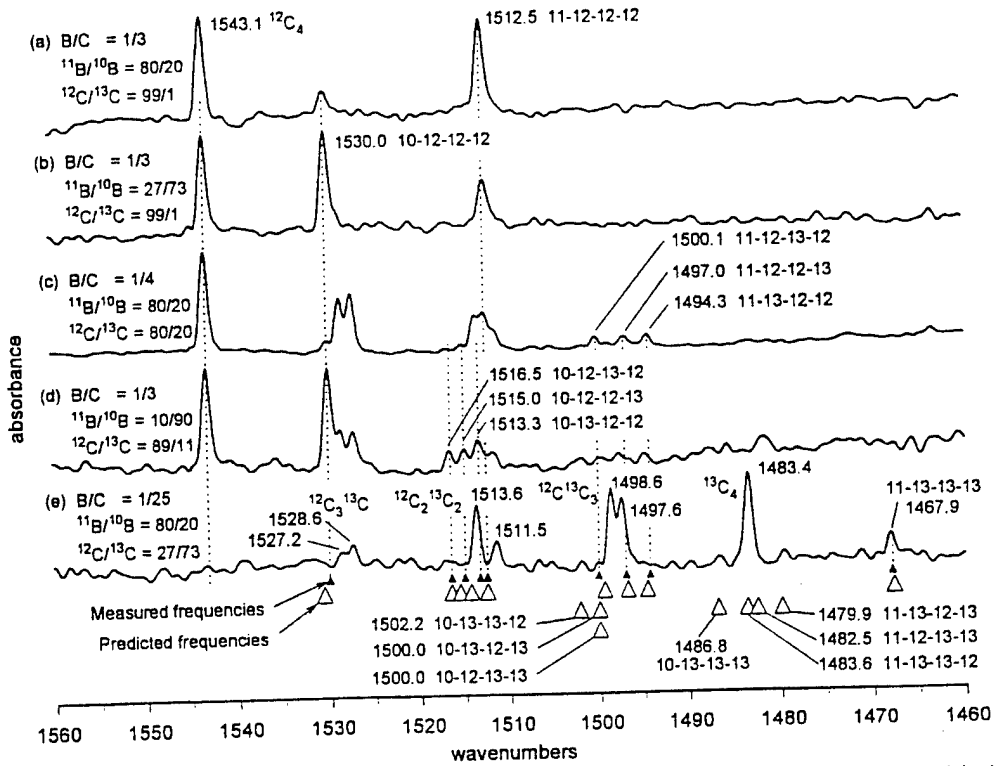


FIG. 1. FTIR spectra of the $\nu_2(\sigma)$ mode of isotopomers of linear BC_3 and the $\nu_3(\sigma)$ mode of isotopomers of linear C_4 . The spectra were recorded at 10 K after annealing the matrices with the indicated compositions at 27.5 K for 150 s. The large open triangles at the bottom show the predicted frequencies of linear BC_3 isotopomers (as explained in the text) and small filled triangles show measured isotopomer frequencies.

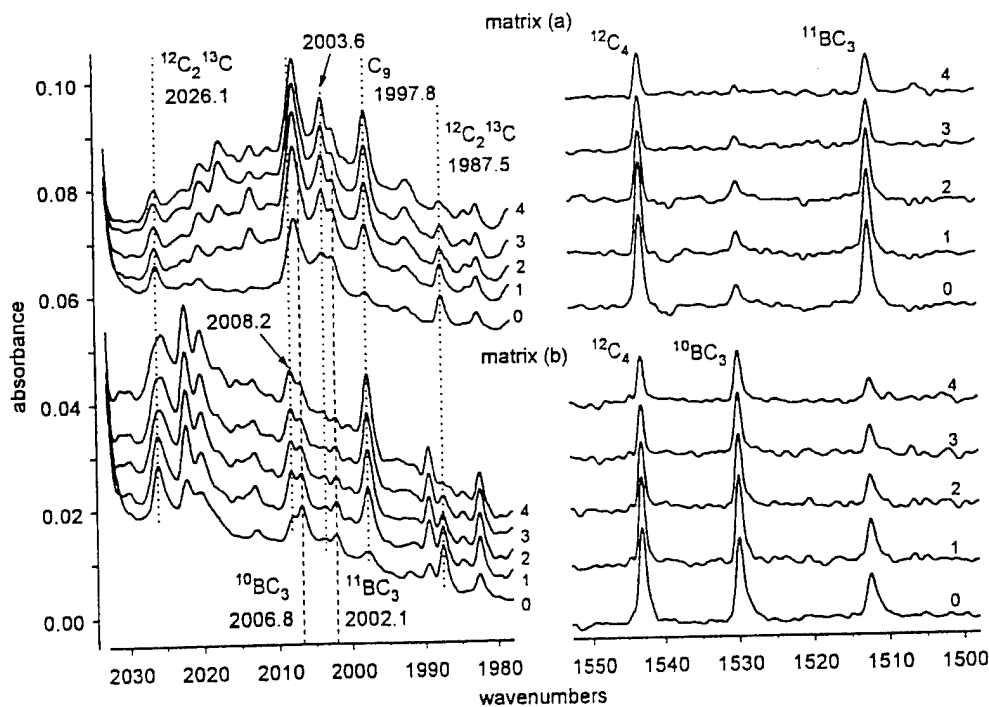


FIG. 2. Spectra obtained from matrix (a) [$^{11}\text{B}/^{10}\text{B} = 4/1$] and matrix (b) [$^{11}\text{B}/^{10}\text{B} = 1/2.7$] showing correlation upon annealing of the $\nu_1(\sigma)$ bands of $^{10}\text{BC}_3$ and $^{11}\text{BC}_3$ at 2006.8 and 2002.1 cm^{-1} with the $\nu_2(\sigma)$ bands at 1530.0 and 1512.5 cm^{-1} . The spectra labeled "0" are from the originally deposited matrix. Labels "1" to "4" indicate spectra recorded after the first through fourth annealing as follows: (1) 27.5 K for 150 s, (2) 30.0 K for 75 s, (3) 32.5 K for 45 s, (4) 35.0 K for 30 s. Frequency and absorbance scales are identical for all spectra. The plotted absorbance is $-\log_{10}$ of the transmittance. To facilitate comparisons between matrices, the absorbance of the matrix (b) spectra are multiplied by 1.4.

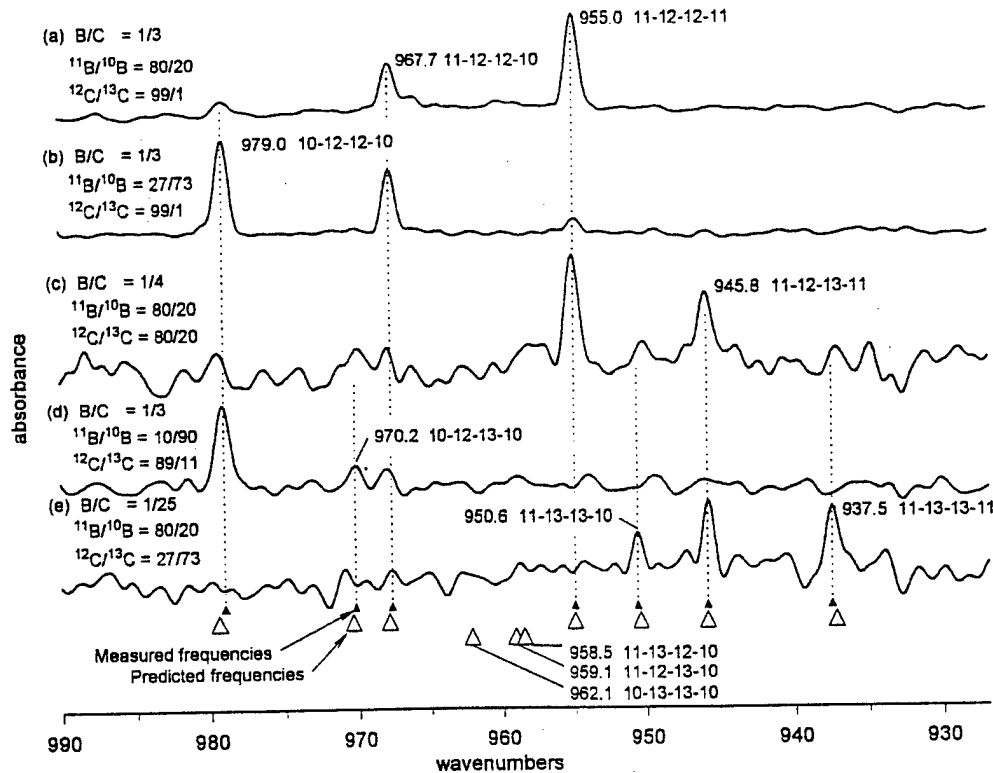


FIG. 3. FTIR spectra of the $\nu_3(\nu_w)$ mode of isotopomers of linear BCCB. The spectra were recorded after annealing the matrices with the indicated compositions at 27.5 K for 150 s. The large open triangles at the bottom show the predicted frequencies of linear BCCB isotopomers (as explained in the text) and small filled triangles show measured isotopomer frequencies.

TABLE IV. Experimental B_2C_2 isotopomer frequency patterns. Frequencies and frequency intervals (cm^{-1}) in triplet bands of B_2C_2 isotopomers.

Boron isotope triplets				Carbon isotope triplets			
Isotopomer	Freq.	Intervals		Isotopomer	Freq.	Intervals	
		Short	Long			Short	Long
$^{10}B_2^{12}C_2$	979.0			$^{10}B_2^{12}C_2$	979.0		
$^{10,11}B_2^{12}C_2$	967.7	11.3	24.0	$^{10}B_2^{12,13}C_2$	970.2	8.8	(16.7)*
$^{11}B_2^{12}C_2$	955.0	12.7		$^{10}B_2^{13}C_2$	(962.3)*		
$^{10}B_2^{12,13}C_2$	970.2			$^{10,11}B_2^{12}C_2$	967.7		
$^{10,11}B_2^{12,13}C_2$	(958.7)*	(11.5)*	24.4	$^{10,11}B_2^{12,13}C_2$	(958.7)*	(9.0)*	17.1
$^{11}B_2^{12,13}C_2$	945.8	(12.9)*		$^{10,11}B_2^{13}C_2$	950.6		
$^{10}B_2^{13}C_2$	(962.3)*			$^{11}B_2^{12}C_2$	955.0	9.2	
$^{10,11}B_2^{13}C_2$	950.6	(11.7)*	(24.8)*	$^{11}B_2^{12,13}C_2$	945.8	8.3	17.5
$^{11}B_2^{13}C_2$	937.5	13.1		$^{11}B_2^{13}C_2$	937.5		

*Frequencies and intervals in parentheses were interpolated or extrapolated from measured quantities.

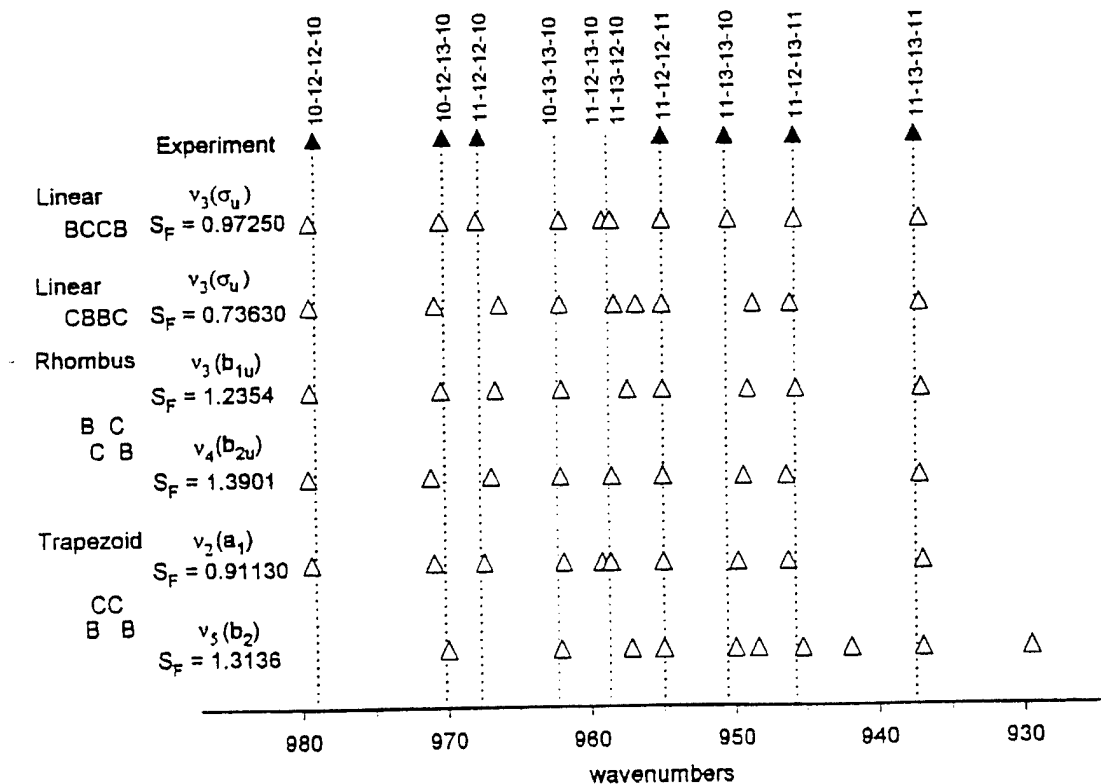
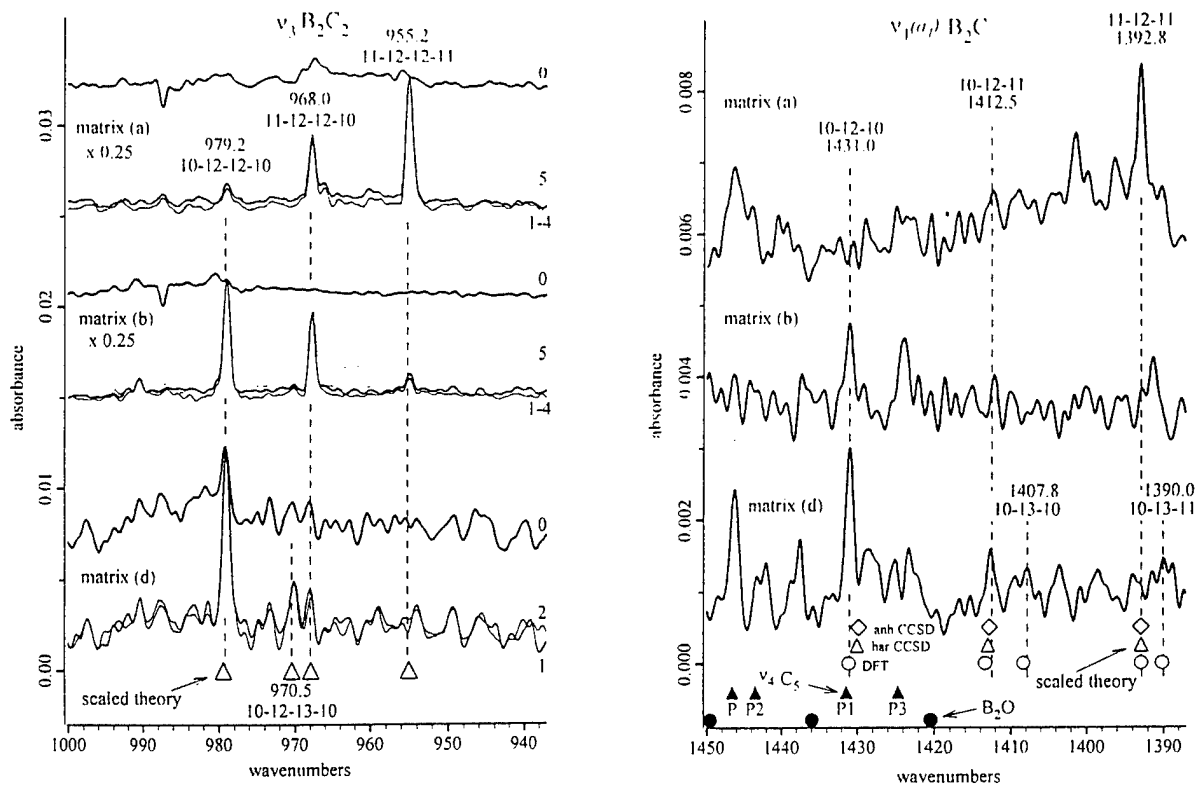
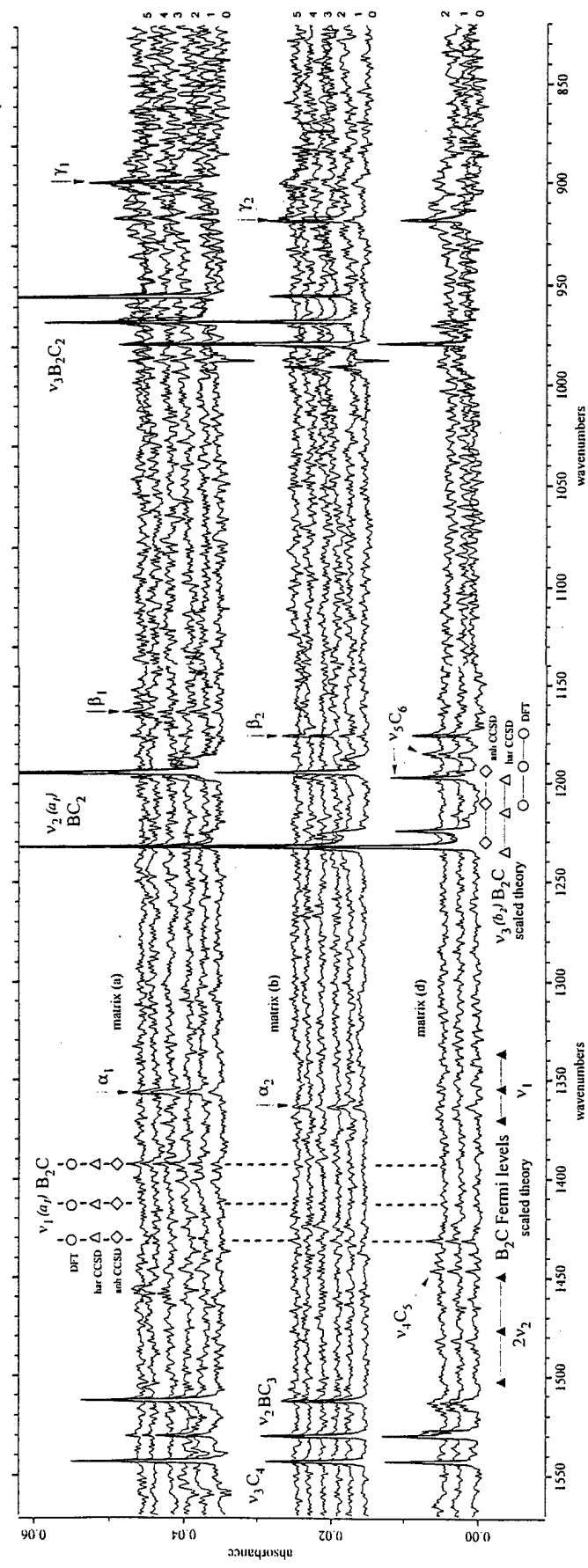
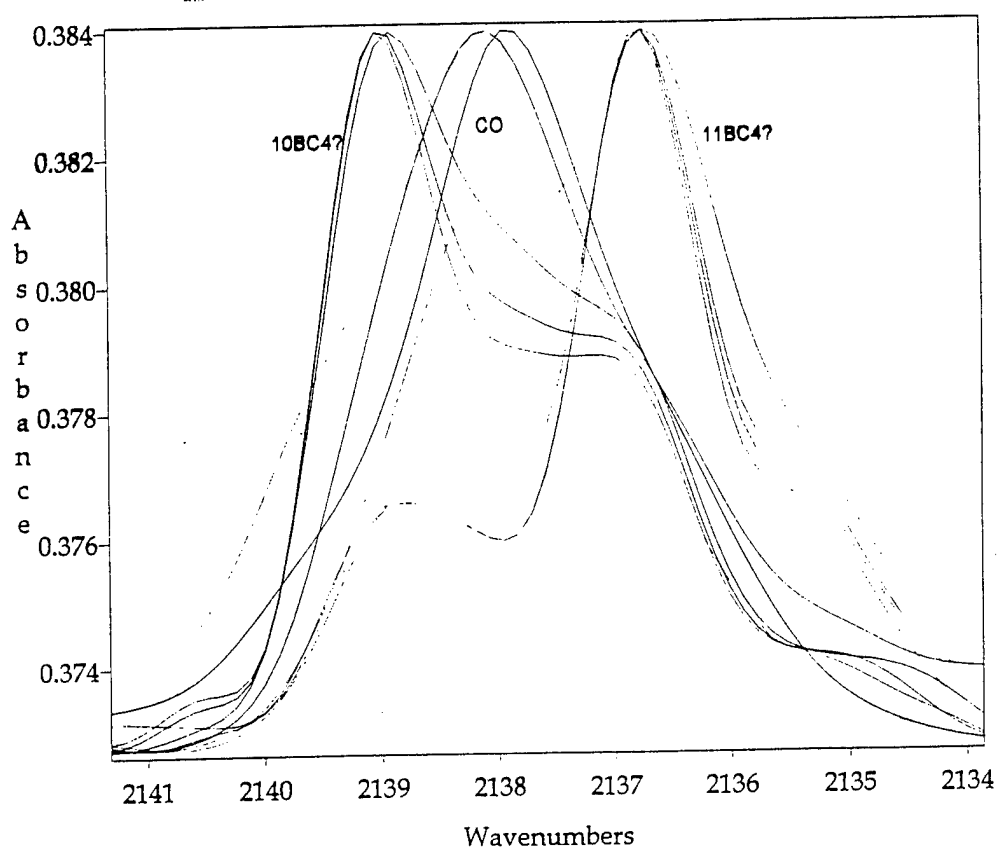
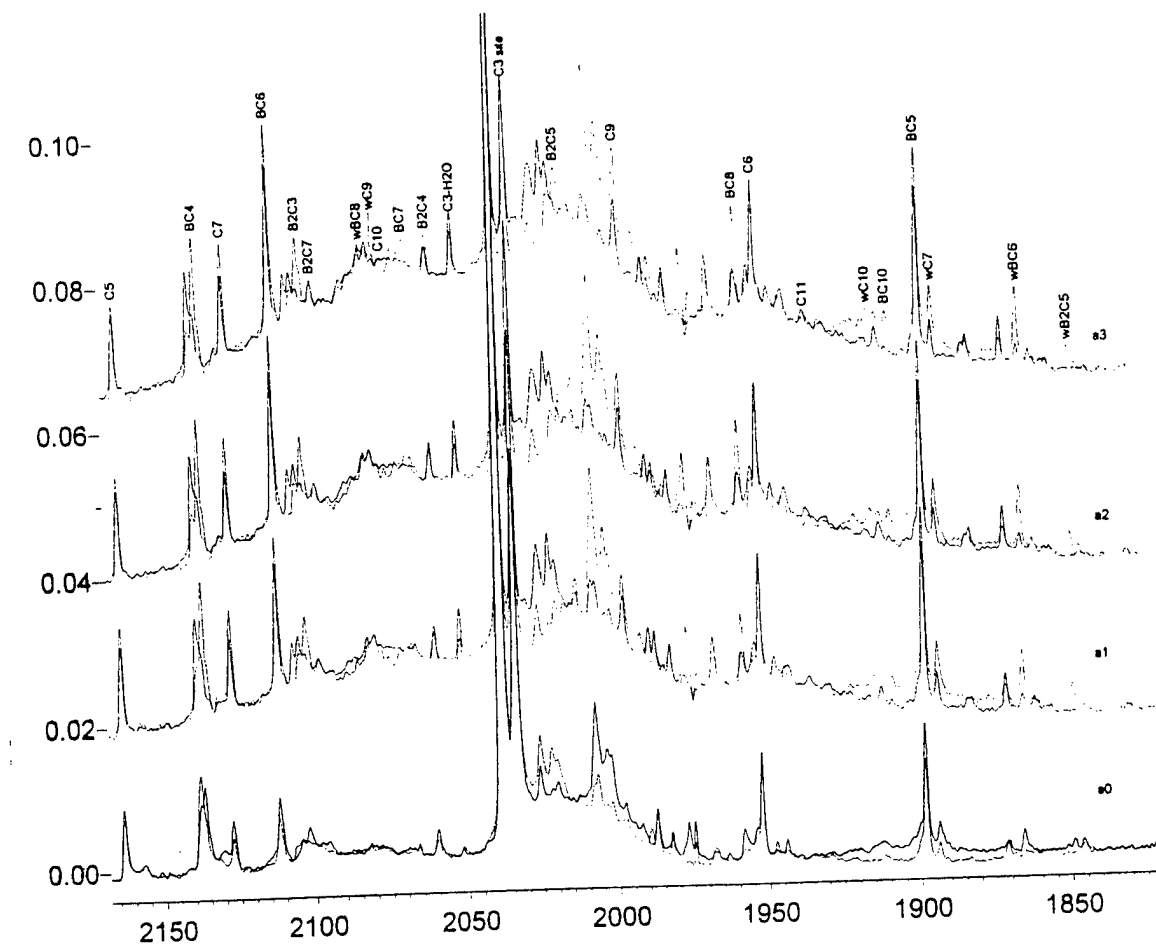
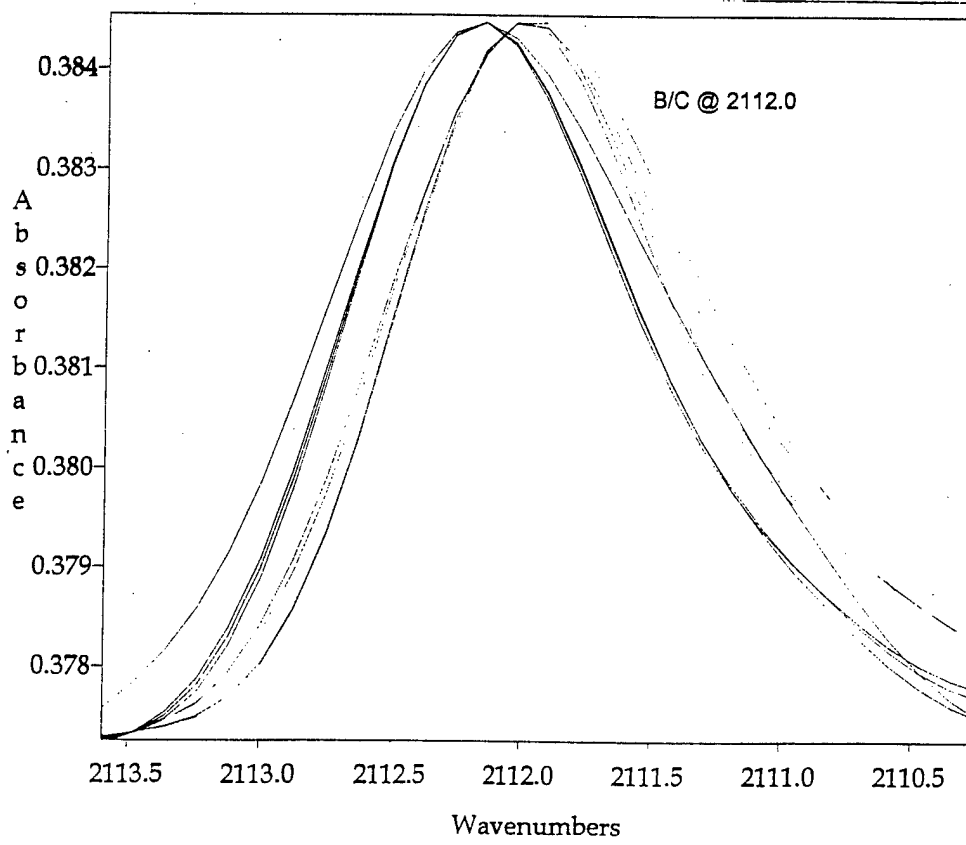
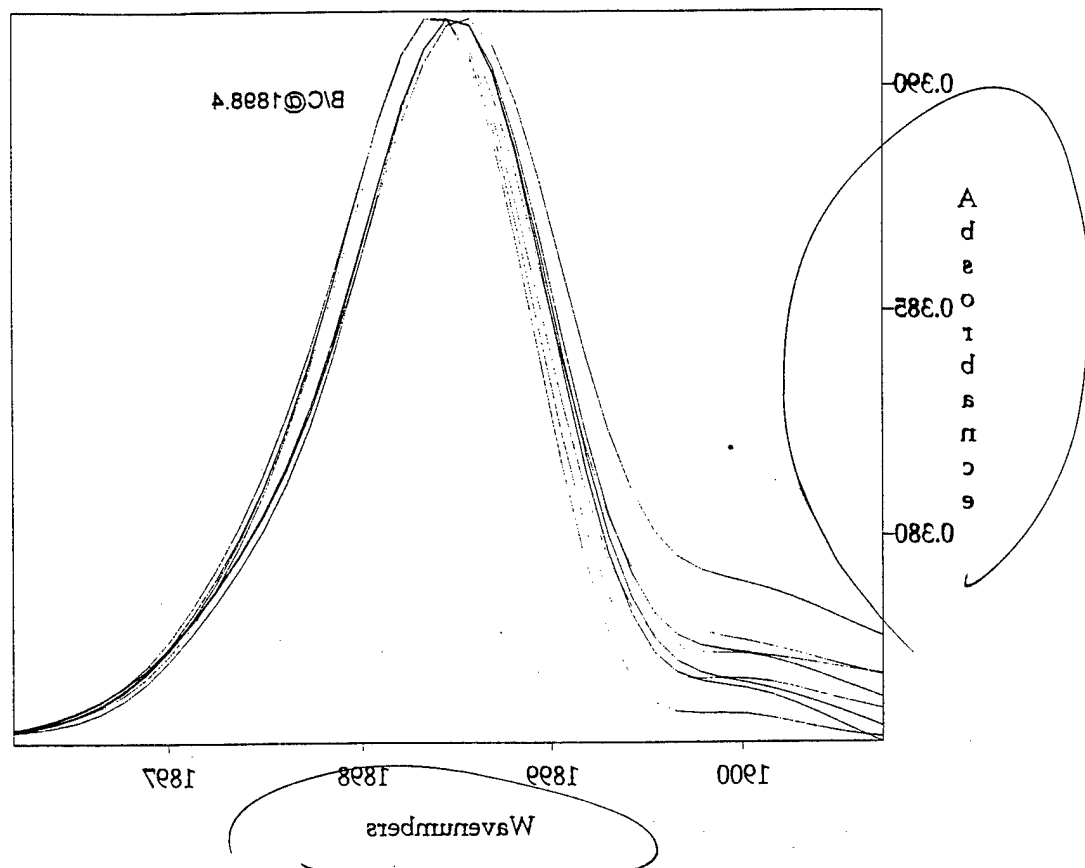


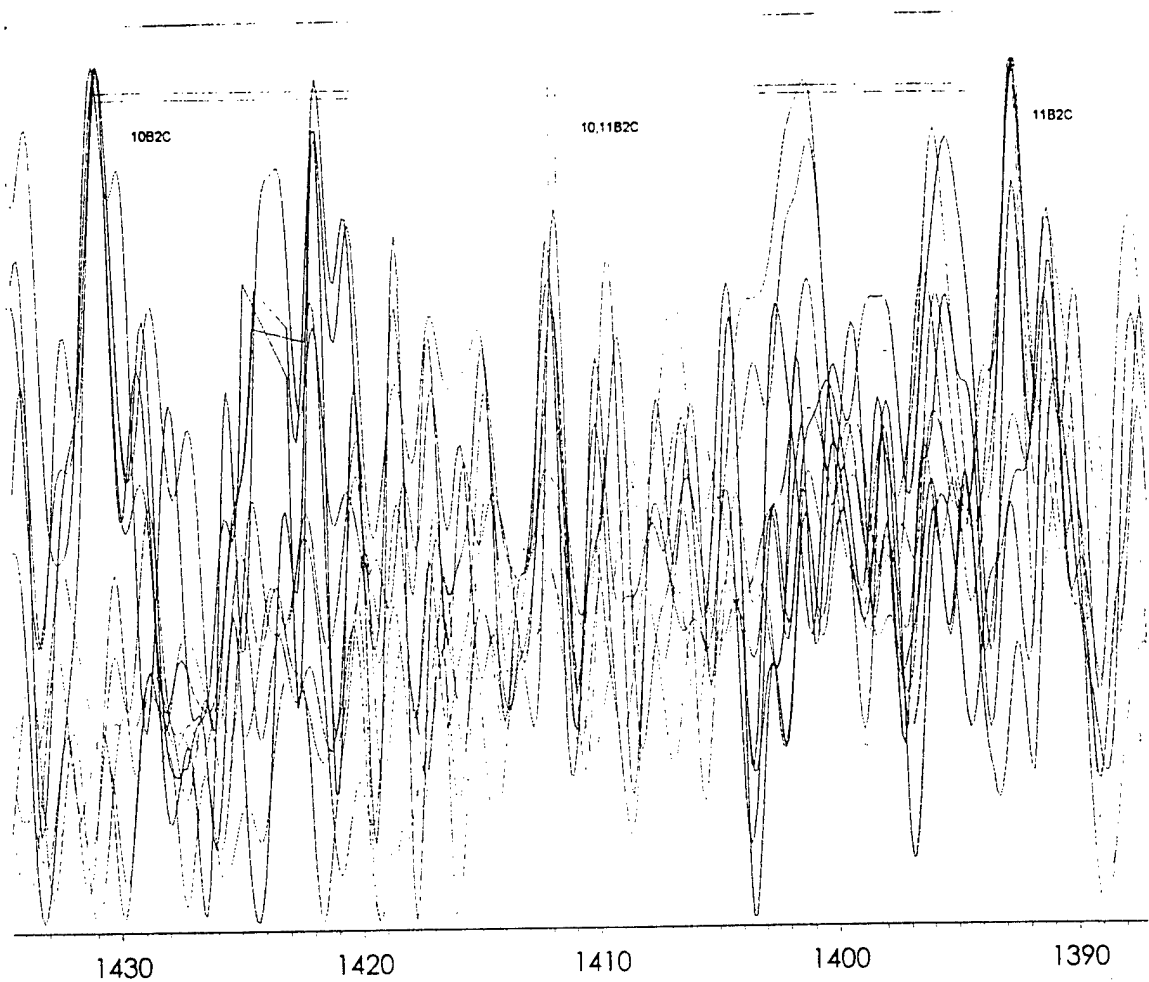
FIG. 4. Comparison of experimental isotopomer frequencies to scaled theoretical isotopomer frequencies for the most intense modes of four B_2C_2 geometries as calculated by Rittby, Ref. 5.

20









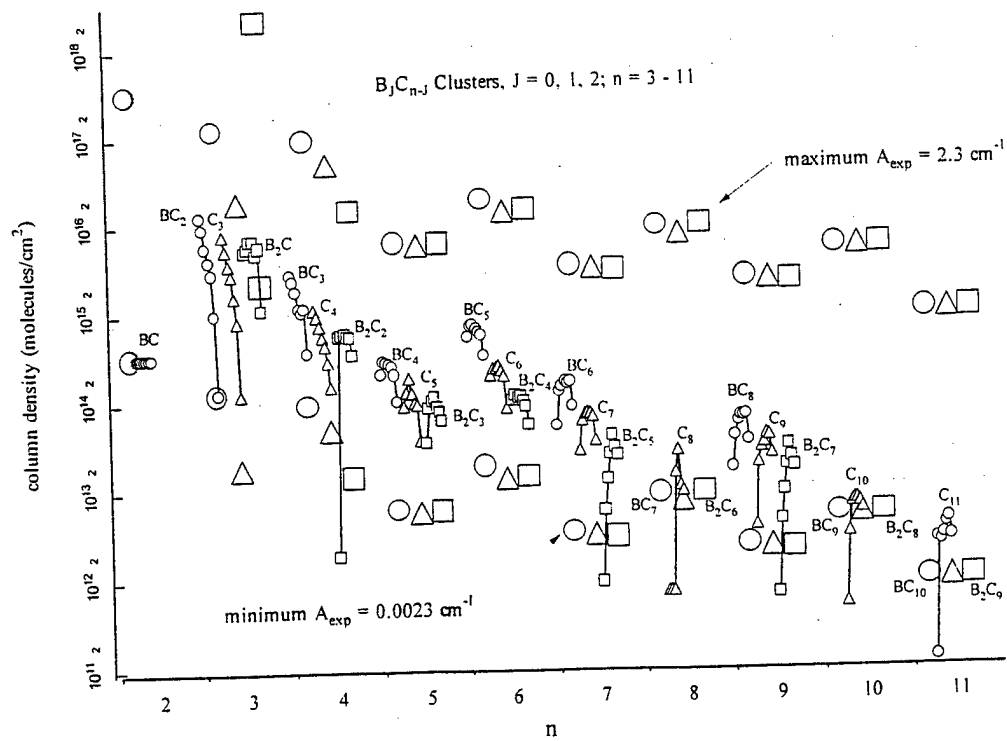
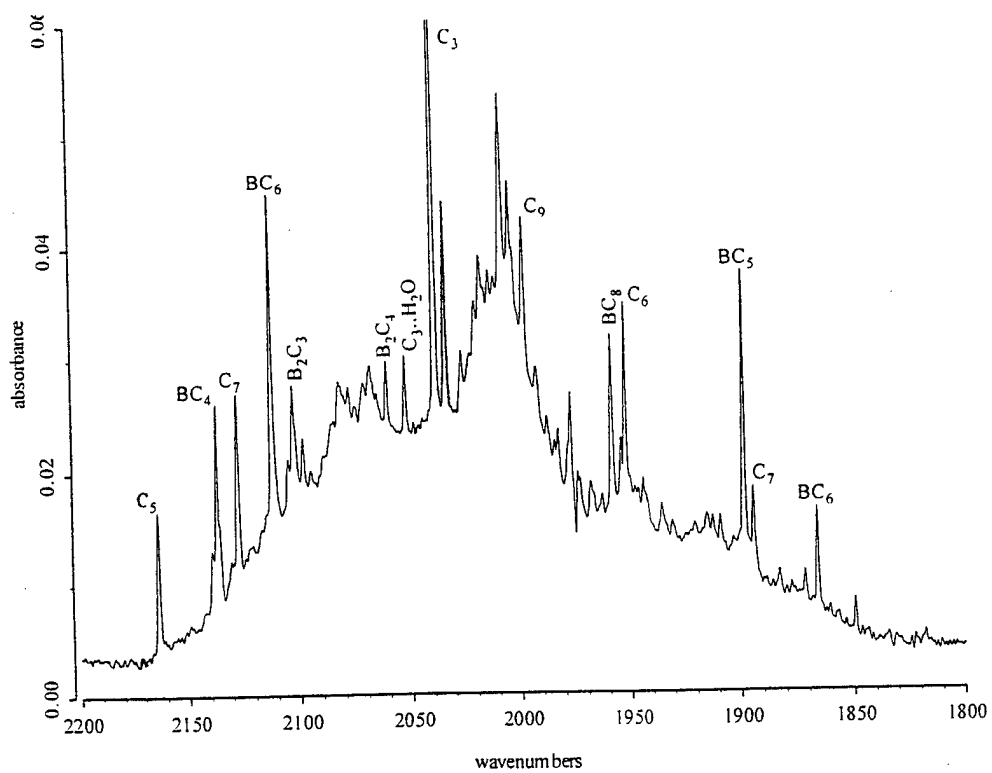


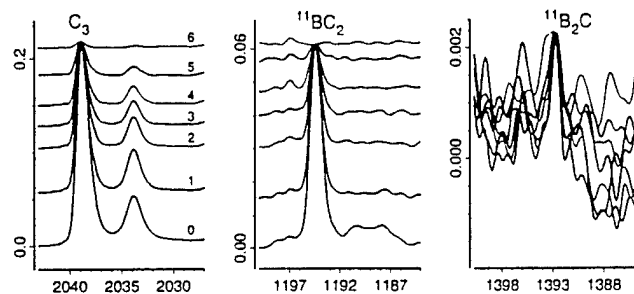
Figure 1. Distribution of B_jC_{n-j} clusters, $J = 0, 1, 2$; $n = 3 - 11$. Circles, triangles and squares represent BC_{n-1} , C_n and BC_{n-2} clusters, respectively. Large symbols denote upper and lower limits of measurement, based on a nominal minimum measurable absorbance of 0.0023 cm^{-1} , and a maximum absorbance for linearity of Beer's law of 2.3 cm^{-1} (1% transmittance. Small symbols denote measured quantities in the initial matrix, and in six annealed matrices. Annealing temperatures and times were (1) $27.5 \text{ K}/150 \text{ s}$, (2) $30.0 \text{ K}/75 \text{ s}$, (3) $32.5 \text{ K}/45 \text{ s}$, (4) $35.0 \text{ K}/30 \text{ s}$, (5) $37.5 \text{ K}/20 \text{ s}$, (6) $40.0 \text{ K}/20 \text{ s}$. The decreases in column density in the fifth and sixth annealing are due to matrix sublimation. Some of the larger clusters ($n = 8, 10, 11$) have not been identified, BC_7 , B_2C_6 , BC_8 , B_2C_8 , BC_{10} , B_2C_9 .

$\omega = 0$ 1 2

matrix (a): $^{11}\text{B}/^{10}\text{B} = 80/20$, $^{12}\text{C}/^{13}\text{C} = 99/1$

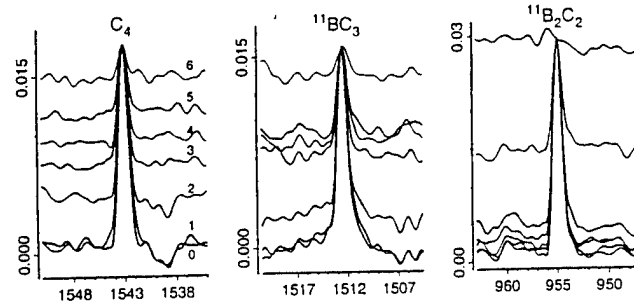
$n = 3$

annealing
0
1
2
3
4
5
6



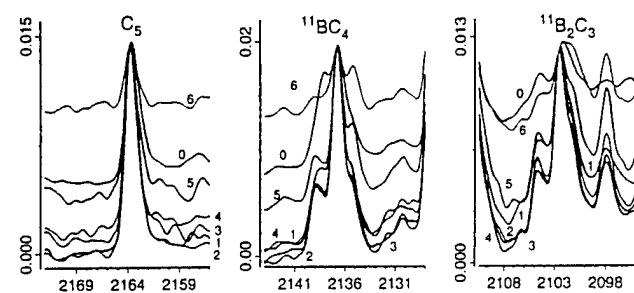
4

annealing
0
1
2
3
4
5
6



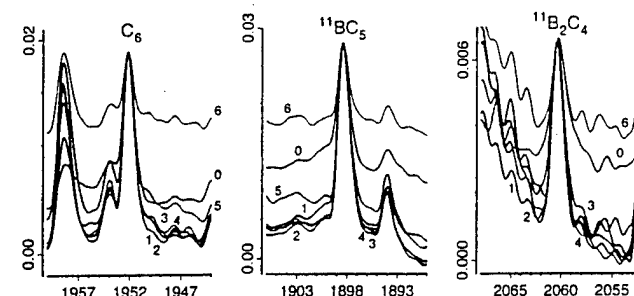
5

annealing
0
1
2
3
4
5
6



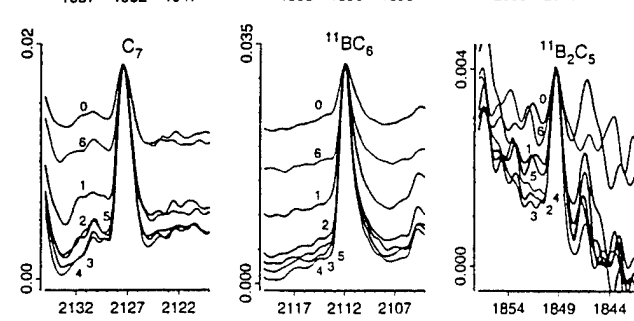
6

annealing
0
1
2
3
4
5
6



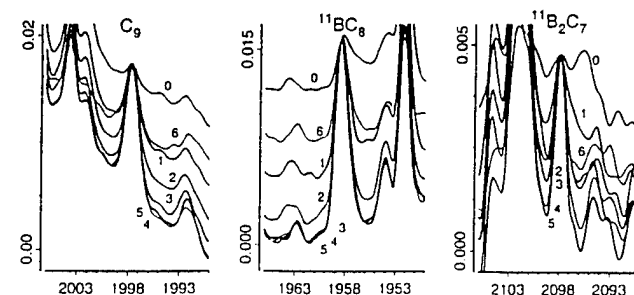
7

annealing
0
1
2
3
4
5
6



8

annealing
0
1
2
3
4
5
6



26

Conclusions

Linear C_3 , cyclic BC_2 , and cyclic B_2C , constituted about 80% of the total observable boron and carbon in the initially deposited matrix, but B_3 was not observed.

The measured trimer distribution in the initially formed matrices was

$$\rho(C_3) : \rho(BC_2) : \rho(B_2C) : \rho(B_3) \sim 1 : 1.5 : 0.5 : < 0.05.$$

Statistical substitution of J boron atoms into an n -atom carbon cluster produces a distribution given by $\rho(BC_{n-J}) / \rho(C_n) = [\{n(n-1)\dots(n-J+1)\}/J!] [B/C]^J$. With the experimental $B/C \sim 1/3$, the statistical trimer distribution is

$$\rho(C_3) : \rho(BC_2) : \rho(B_2C) : \rho(B_3) \sim 1 : 1 : 0.33 : 0.03.$$

Agreement between distributions implies trimers form by random condensation of well-mixed atoms, uninfluenced by the relative energies of the trimers, the energies of their precursors, or preferential kinetics pathways that could otherwise distort the statistics.

Linear C_3 and cyclic BC_2 , disappeared entirely when the matrices were repeatedly annealed to temperatures between 25 K and 35 K, but cyclic B_2C was inert.

Linear C_4 and BC_3 (BCCC) disappeared more slowly, and linear B_2C_2 (BCCB) grew to $\sim 95\%$ of its final value during the first annealing. B_2C_2 was also inert, as B_2C .

The sources of B_2C_2 are from condensation of atom plus trimer ($B + BC_2$ but not $C + B_2C$) or dimer + dimer ($BC + BC$ but not $B_2 + C_2$). Although BC was not observed, the upper limit of $\rho(BC)$ is larger than $\rho(B_2C_2)$ so that BC cannot be ruled out as a source of B_2C_2 .

The growth of B_2C_2 is conclusive evidence of the presence of BC and/or B in the originally deposited matrix in an amount at least as great as the growth of B_2C_2 .

Linear C_5 , BC_4 (BCCCC) and B_2C_3 (BCCCB) and larger linear clusters (BC_{n-J} , $5 < n < 11$, $J = 0, 1, 2$), all grew upon annealing.

The sources of B_2C_3 are dimer + trimer ($BC + BC_2$ but not $B_2 + C_3$) and atom + tetramer ($B + BC_3$ but not $C + B_2C_2$).

Since $\rho(BC_2) \sim 5\rho(BC_3)$ in the initially deposited matrix, the $BC + BC_2$ source is dominant. Growth of B_2C_3 conclusively establishes the presence of BC in the matrix in an amount at least as great as the amount by which B_2C_3 grows.

Growth of BC_4 occurs primarily by $BC + C_3$ rather than $B + C_4$ or $C + BC_3$ because $\rho(C_3) \sim 10\rho(C_4)$ and $\rho(C_3) \sim 2\rho(BC_3)$. Growth of C_5 occurs by $C + C_4$ and $C_2 + C_3$, which establishes the presence of C and/or C_2 in the original matrix in an amount at least as great as C_5 growth.

Disappearance of triangular BC_2 requires breaking of one of its B-C bonds when one of its carbon atoms is attacked. The major reorganization of electronic energy involved in opening the ring appears to occur with little ($< \sim 3$ kcal mol⁻¹) or no energy barrier, which makes this small molecule a candidate for an interesting *ab-initio* study of unusual reactivity at low temperature.

Conclusions

1. C_3 is linear but BC_2 , B_2C and B_3 are cyclic.
2. $n > 3$; $J = 0, 1, 2$ clusters are linear. Boron atoms cap the ends of linear chains.
3. $J = 0, 1, 2$ substitution in $n \geq 5$ clusters does not significantly affect IR intensities.
4. For $n \geq 5$ the absorption intensity of even n clusters is two to three times smaller than that of odd n clusters.
5. B_2C_2 grew most dramatically upon annealing. BC was not detected. Its upper limit column density is comparable to that of $n = 4$ clusters. B_2C_2 sources may be $2BC$ or $B + BC_2$ but $C + B_2C$ does not form B_2C_2 .
6. $n = 3, 4$; $J = 0, 1$ clusters disappear upon annealing but $J = 2$ clusters either grow or remain unchanged. Capping the ends of clusters with boron seems to render them inert to further condensation.
7. Statistical cluster distributions are apparent in $n = 4$ and 5 clusters. B_2C yields are too high and B_2C_{n-2} yields are too low in larger $n \geq 6$ clusters.
8. $n \geq 5$ clusters grow upon annealing and larger clusters grow more than smaller clusters.

Conclusions from Carbon HEDM Research

Quantitative analysis - Establishes HEDM density, distribution of carbon clusters, heat of formation of HEDM. Enables tracking of growth and decay of carbon clusters - carbon bookkeeping - quantification of "invisible carbon", C-atom and C_2 .

Highest density matrix (equivalent C-atom density ~ 1 mole percent in argon) contained 40% "invisible" carbon (C, C_2), determined by tracking the growth of the "visible" (measurable) carbon to a constant composition after repeated annealing. Main product of condensation is cyclic C_6 .

Yields of cyclic- C_6 are a factor of two larger than the combined yield of all other clusters in the fully condensed, highest density matrices. Cyclic- C_6 is the dominant condensation product.

Knudsen oven produces $\sim 80\%$ C_3 and $\sim 10\%$ each of C_2 and C-atom (by mass).

Laval oven with $\Delta T \sim 600$ K (between graphite surface and orifice) produces $\sim 5\%$ C_3 and C_2 and $\sim 90\%$ C-atom. C-atoms production by our oven (relative to C_3) is enhanced by higher temperature, which is accompanied by higher ΔT .

Substrate must be shielded from oven to prevent condensation during deposition.

Higher temperature oven places higher heat load on substrate, which promotes condensation.

Obtained higher density matrices by decreasing argon flux and maintaining oven flux. However, condensation was also increased.

One experiment with argon/5% H_2 caused nearly complete loss of C_{n+1} and C_{n+2} relative to C_{n+3} , suggesting that H_2 scavenges C-atoms efficiently during co-deposition.